1

Fundamental Concepts

1.1 Introduction to Nanoscience and Nanotechnology

The word "nano" originated from the ancient Greek νᾶνος (nânos), meaning dwarf. In modern science and technology, nano is specifically used as an SI prefix, referring to the multiplying factor of 10^{-9}. For example, an anti-HIV/AIDs drug can be said to give an inhibitory concentration of a few nanomoles per liter (10^{-9} mol L^{-1}), an organic fluorescent molecule shows a fluorescence lifetime of tens of nanoseconds (10^{-9} second), and the third carbon allotrope, Buckminsterfullerene C_{60} (bucky ball), has a diameter of 1 nanometer (10^{-9} meter) as illustrated in Figure 1.1. Today the use of "nano" has gone far beyond its numerical meaning. In the academic world, nano has become a buzzword spanning the fields of chemistry, physics, biology, medicine, and engineering, where it is used to describe studies of advanced molecular, macromolecular, and supramolecular materials with the dimension of nanometers. In the industrial sector, many nanotechnology companies have been established to deal with the development and commercialization of nanometer-sized materials and devices for special purposes and tasks. The National Nanotechnology Initiative (NNI) in the US has defined nanotechnology as a science, technology, and engineering conducted at the scale of 1—100 nm. Unique properties and functions would arise from materials on such a small scale, which are often unprecedented and considerably more advantageous in comparison to conventional bulk materials.

So, how did nanotechnology start? The production and manipulation of nanoscale materials in fact have a surprisingly long history. Take the famous ancient artifact, the *Lycurgus cup*, as an example. This cup is an impressive Roman treasure made in about AD 400, which was named for its depiction of King Lycurgus of Thrace entangled in grape vines. The *Lycurgus cup* is well known because of its color-changing glass. When light is shone upon it, the cup displays

Organic Nanochemistry: From Fundamental Concepts to Experimental Practice,
First Edition. Yuming Zhao.

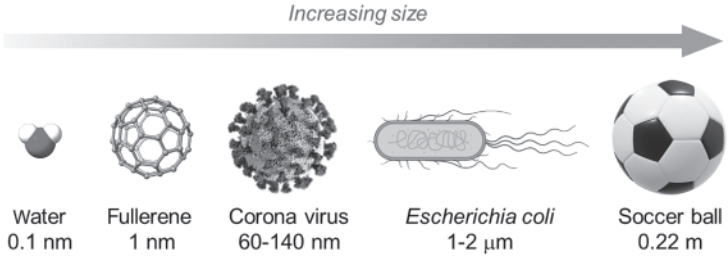

Figure 1.1 Illustration of various objects at the meter, micrometer, and nanometer scales. Credit: Alissa Eckert, MS; Dan Higgins, MAM / Wikimedia Commons / Public Domain.

a jade green color. When light is shone through it, however, the cup turns into a brilliant red color. The reason for this color-changing property is due to the gold–silver alloyed nanoparticles that are distributed in the glass. These nanoparticles scatter reflected light and back-illuminated light in different ways. Another example of ancient nanotechnology is the *Damascus steel swords* from the Middle East, which were made between AD 300 and AD 1700. They are known for their superior strength, shatter resistance, and exceptionally sharp cutting edge, owing to the use of the so-called wootz steel in their blade making. A recent scientific discovery disclosed that the wootz steel is full of carbon nanotubes, which are a class of appealing nanomaterials discovered by scientists in 1991. Nowadays, those artifacts would be included in a sub-branch of nanotechnology, known as nanocomposites. Beyond a doubt, those ancient artisans possessed masterful skills and empirical knowledge which enabled them to fabricate such stunning artifacts, but the presence and roles of the nanomaterials were not consciously known by them, neither were their related chemical and physical principles.

Many consider that the year of 1959 marked the inception of the concept of modern nanotechnology. In the December of that year, a visionary American physicist, Richard Feynman, who was the Nobel Prize laureate in Physics in 1965, gave a lecture at an annual meeting of the American Physical Society at Caltech, entitled *There's Plenty of Room at the Bottom* [1]. In this famous lecture, Feynman envisioned a day when devices and machines could be miniaturized in such a way that huge amounts of information could be stored in extremely small spaces, while machines could be fabricated and compacted together at a much smaller scale. Feynman's futuristic ideas sparked the beginning of the modern nanotechnology, although Feynman himself never used the term "nanotechnology" in his lectures. It was Prof. Norio Taniguchi of the Tokyo University of Science who coined the term "**nano-technology**" fifteen years later. In 1974, Taniguchi published a paper entitled *On the Basic Concept of Nanotechnology*, in which he wrote "Nanotechnology mainly consists of the processes of separation, consolidation, and deformation of materials by one atom or one molecule" [2]. This term was then adopted and greatly promoted by an American engineer, Eric Drexler, in his

popular book *Engines of Creation: The Coming Era of Nanotechnology* published in 1986 [3]. In this book, Drexler imagined numerous future technologies, including an unprecedented class of tiny machines, which he termed **molecular assemblers**. He predicted that these assemblers would have the ability to precisely build objects in an atom-by-atom manner.

The era from 1980s to 1990s was full of exciting experimental discoveries and achievements in nanotechnology. In 1981, Gerd Binnig and Heinrich Rohrer at IBM Zurich Research Laboratories in Switzerland developed the first working scanning tunneling microscope (STM), for which they won the Nobel Prize in Physics in 1986. In 1985, these IBM researchers developed the technique called atomic force microscopy (AFM), which added another powerful tool for imagining and manipulating nanoscale objects on various substrates. A *tour de force* in precise positioning of atoms was achieved by IBM researchers Don Eigler and Erhard K. Schweizer in 1989, who used STM to create a tiny IMB logo with only 35 xenon atoms (see Figure 1.2). A range of nanoscale materials were discovered and developed during this period, which opened many sub-branches in modern nanotechnology.

Nanotechnology is not an individual discipline in science and engineering. Unlike the traditional disciplines (e.g., mathematics, chemistry, physics, and biology), nanotechnology is more like a technological hub that gathers a vast array of research under its umbrella. Research involving nanoscale materials has permeated almost every classical division of science and technology, making it highly multidisciplinary and without a clear boundary. Therefore, it is very hard to define the skills and precise type of backgrounds required to be a "nanotechnologist." Nanotechnology broadly covers engineering, chemistry, biology, medicine, computer science, theoretical simulations, devices and structures fabrication, just to name a few. In most nano-related studies, the preparation of nanoscale materials and precise control over their dimensions and shapes take center stage. To achieve these goals, special methods for nanofabrication are needed. In general, nanofabrication can be carried out using two different approaches, namely **top-down** and **bottom-up**. The top-down approach starts with the manipulation

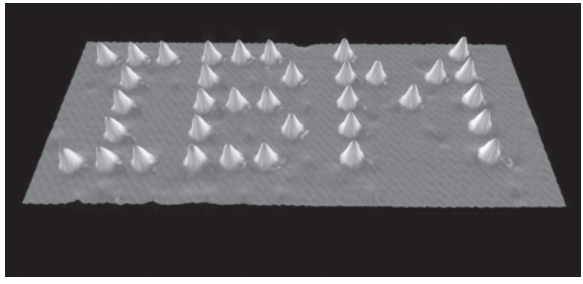

Figure 1.2 An IBM logo formed by positioning 35 xenon atoms on a nickel (110) surface. Credit IBM.

of bulk materials and structures. For example, the fabrication of a computer chip is done by "engraving" the surface of a piece of single-crystal silicon using a technique known as photolithography as the key step. Through the top-down approach, miniaturized devices are "chiseled out" of the bulk material in a precisely controlled manner, with the original integrity of the bulk material (e.g., crystallinity and long-range order) still retained. The bottom-up approach produces nanomaterials and devices through the self-assembly or chemical synthesis of certain nanoscale building blocks. The self-assembling process is dictated by specific chemical and/or physical forces (e.g., metal ligand coordination, hydrogen bonding, and π–π stacking) to form defined nanostructures. The building blocks can be obtained from naturally existing materials (e.g., DNA, lipids, carbohydrates) or prepared by chemical synthesis (e.g., synthetic molecules and polymers). The biological world is full of events utilizing the bottom-up approach, such as protein synthesis and cellular growth. Inspired by these natural materials and events, enormous efforts have been dedicated to applying various molecular functions and supramolecular forces to create nanostructures and materials.

1.2 Nanochemistry in Action

As prophesized by Richard Feynman, *there's plenty of room at the bottom*. Atoms and molecules are at the bottom of our physical world and can be manipulated and controlled. The knowledge and techniques for dealing with the assembly of atoms and molecules have long existed in the field of chemistry. According to the definition provided by Britannica, chemistry is "the science that deals with the properties, composition, and structure of substances (defined as elements and compounds), the transformations they undergo, and the energy that is released or absorbed during these processes". Jean-Marie Lehn, a 1987 Nobel Prize laureate in Chemistry, stated that "the science of chemistry is not just about discovery. It is also, and especially, about creation. It is an art of the complexification of matter. To understand the logic of the latest discoveries in nanochemistry, we have to take a 4-billion year leap back in time". So, it is obvious that chemists have been equipped with the required tools (knowledge of the properties of molecules including their reactions) to design and prepare nanoscale materials from the bottom up.

The intermarriage of chemistry and nanoscience has given rise to the vibrant interdisciplinary area of **nanochemistry**. One of the main focuses of nanochemistry is placed on the design and synthesis of molecular building blocks for the construction of various nanostructures. In this regard, the basic concepts and principles of nanochemistry do not differ too much from those encountered in traditional covalent and non-covalent chemistry. For example, the synthesis of a functional unit in a molecular machine can be achieved through the same bond-forming reactions that are useful in the synthesis of natural products or pharmaceutical compounds. The assembly of a nanoscale supramolecular structure may

utilize the hydrogen bonding interactions in a manner similar to the Watson-Crick base pairing that typically exists in DNA and RNA molecules. What have proven to be more important for nanochemistry are the following: the creation of novel nanomaterials useful for technological applications, the development of new methods for more efficient materials synthesis and better characterization, and the understanding of the performances of nanomaterials at the molecular and supramolecular levels. In this respect, the existing chemical and biological literature is of great value for nano researchers to learn from and to be inspired.

Over the past few decades, nanochemistry has yielded fruitful results that have made profound impacts in our everyday lives and social development. Many advanced nanoscale organic and inorganic materials have found applications in the fields of advanced electronics and optoelectronics. New nanoelectronic materials are being used to replace the traditional conducting and semiconducting materials for improved device performances. For example, carbon nanotubes can be used in the fabrication of flexible displays and stretchable electronic devices through printing methods. Graphene serves as a robust and transparent electrode material in the production of new-generation touch screens. In the food industry, nanostructured materials have already been used for food packaging, functional food development, food safety, and shelf-life extension of food products. In solar energy technology, the use of nanoparticles such as quantum dots has helped to achieve enhanced absorption and sunlight energy capture, resulting in the development of solar cells that perform more efficiently. Nanoparticles such as titanium oxide (TiO_2) can be coated on the surface of glass panels or other solid substrates to form self-cleaning nanocoatings. Photocatalytic reactions enable such nanoparticles to clean dirt and grime on the surface. In a similar way, functional nanoparticles have been designed and engineered to act as efficient photocatalysts for water splitting, producing hydrogen as a clean energy source. Nanotechnology has also made significant impacts in environmental control and remediation. For instance, toxic organic pollutants in wastewater can be conveniently degraded under sunlight with the aid of photocatalytic nanoparticles. Nanoadsorbents can effectively remove toxic heavy metals from wastewater. In the field of medicine, nanomaterials have been widely used in diagnosis, controlled drug delivery, and regenerative medicines. For example, polymer-based nanocontainers are designed to show responses to external stimuli (temperature changes, light, ultrasound), which trigger the release of diagnostic molecules or drugs carried inside when they reach the targeted tissues or cells. Recently, "nanobots" have been fabricated to serve as miniature surgeons to repair damaged cells and modify intracellular structures in a highly precise manner. Such technology is expected to revolutionize the therapeutic methods for chronic diseases such as cancer. Even our daily lives have felt the benefits of nanochemistry. For example, smart nanocoated fabrics have been developed to exhibit amazing resistance to water, stain, and wrinkling. Nanocomposite materials have allowed sports equipment to be stronger, lighter, and more durable.

1.3 Structures and Covalent Bonding of Organic Compounds

1.3.1 Localized Covalent Bonds and Lewis Structures

In the molecular world, the distribution of electrons in molecules plays a vital role in controlling the structural, physical, and chemical properties of molecule-based materials. So, it is essential to establish a deep level of understanding of this quintessential property prior to carrying out various kinds of chemical research. **Lewis structures** are a simple and powerful approach to describe the structures of molecules, particularly organic molecules. The concept was first formulated by G. N. Lewis in 1916, who proposed that chemical bonds resulted from the sharing of electron pairs between atoms [4]. For the second-row atoms, Lewis stipulated that the most stable structures possess eight valence shell electrons, known as the **rule of eight** or **octet rule**. Following this rule, Lewis structures containing second-row atoms with more than eight valence electrons are considered too unstable to exist, and therefore should be avoided in the structural drawing.

Figure 1.3 illustrates the Lewis structures for various molecules containing second-row atoms and hydrogens. It can be seen that covalent bonds are drawn as lines, each of which represents a pair of shared valence electrons. Non-bonding valence electrons are drawn as either a pair of dots to represent an electron lone pair or a single dot for a free radical center. Positive and negative formal charges need to be assigned to cationic, anionic, and charge-separated species. The rules for drawing Lewis structures are not derived from rigorous quantum theories; however, they serve as an intuitive and powerful tool to account for electrons and charges in molecules. Straightforward pictures of electron distribution in molecules can be perceived from the Lewis structures.

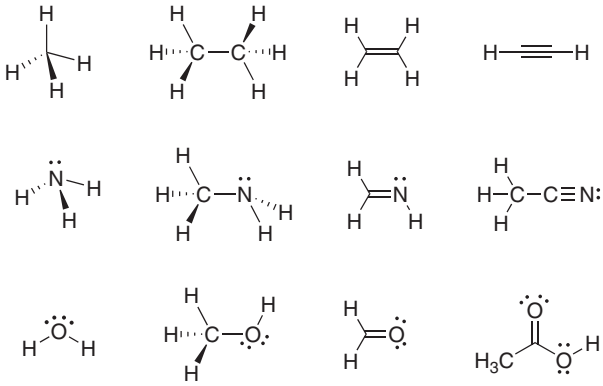

Figure 1.3 Lewis structures of simple molecules containing hydrogen, carbon, nitrogen, and oxygen atoms.

One major limitation of the Lewis structures is that they cannot provide information about the geometry of the molecules they depict (e.g., the molecular shapes and spatial arrangements of their constituent atoms). Nevertheless, this deficiency can be compensated by applying the **valence shell electron pair repulsion** (VSEPR) theory [5–7]. The VSEPR (pronounced "vɛspər") theory is based on the consideration of the Pauli Exclusion Principle and electrostatic repulsion of valence electrons (Coulomb's Law). Simply put, valence electron pairs in a molecule repel one another, and the stable structure of a molecule is a result of the minimization of these repulsions. The repulsion model can be readily applied to the AX_n type of molecular systems to predict the geometries as outlined in Figure 1.4. Herein, A is a central atom that is covalently bonded to several ligands (X_n). Assuming that there are no nonbonding electron pairs present, so only the A–X bonds contribute to the electrostatic repulsion within the system. If we treat each of the A–X bond as a point charge, the optimal arrangement of an AX_n system can be predicted using a model of charges on a sphere. As shown in Figure 1.4, to obtain the minimum mutual charge repulsion, the geometric outcomes for AX_n systems should be linear (n = 2), trigonal planar (n = 3), tetrahedral (n = 4), trigonal bipyramidal (n = 5), and octahedral (n = 6).

With the aid of the VSEPR theory, the geometry of simple organic molecules can be readily predicted. As shown in Figure 1.5, the molecule of carbon dioxide (CO_2) is predicted to take a linear shape, considering the electrostatic repulsion occurring between the two sets of C=O bonds. In a similar way, the geometries of borane (BH_3) and methane (CH_4) are predicted to take a trigonal planar and a tetrahedral shape, respectively. As a result, the bond angles in these two molecules are 120° and 109.5°, respectively. If we take steric effects into consideration, the experimentally observed bond angles which are slightly deviated from the ideal VSEPR predicted geometries can be reasonably explained. For example, the

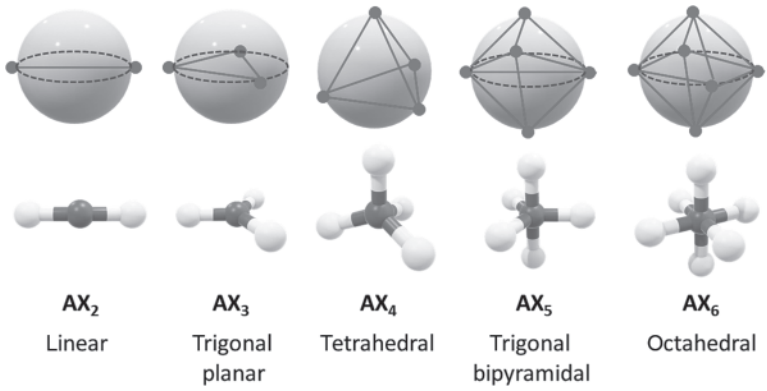

Figure 1.4 Predicted geometries for various AX_n systems according to the VSEPR theory.

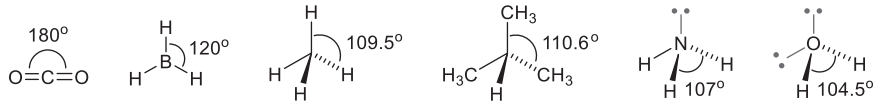

Figure 1.5 Bond angles in various simple molecules.

C–C–C bond angle in isobutane is determined to be 110.6°, which is slightly larger than the angle of 109.5° for an ideal tetrahedral arrangement. This outcome can be explained by that the repulsion between two C–C bonds is greater than that between a C–H bond and a C–C bond, since the methyl group is bulkier than hydrogen. If non-bonding electron lone pairs are present in the valence shell of a molecule, they should be counted as a repulsive domain similar to a covalent bond. Note that the lone pair electrons are distributed closer to the nucleus than the bonding electron pairs. As such, they tend to give stronger repulsion to adjacent electron pairs than the bond electron pair does. The repulsive forces in a molecule thus show a decreasing trend as follows: lone pair–lone pair > lone pair–bond pair > bond pair–bond pair. These notions can be applied to better rationalize the molecular geometries of ammonia (NH_3) and water (H_2O), where the H–N–H and H–O–H angles are 107° and 104.5°, respectively.

Besides using Lewis structural formulas and VSEPR theory, molecular structures can be more accurately predicted through quantum mechanics (QM) calculations. One classical approach that was rooted in the notion of electron pair bonding is called the **valence bond** (VB) theory [8]. In 1927 Heitler and London applied this method to calculate the molecule of dihydrogen. Their results indicated that the two hydrogen nuclei show a certain distance at an energy minimum, with electron density accumulated in between them. In fact, the VB theory gave rise to the notions of covalent bonds that are equivalent to the theory of electron pair sharing proposed by G. N. Lewis. Further application of the VB theory to simple molecules, particularly those containing second-row elements, led to the concept of **hybridization**. Linus Pauling developed this concept by mathematically mixing atomic orbitals together and then dividing the sum into equivalent parts [9]. Each part is called a **hybrid orbital**. Using the hybridization model, the structures and orbital properties of molecules can be conveniently interpreted. For example, in methane molecule (Figure 1.6) the central carbon atom has its four atomic orbitals (2s, $2p_x$, $2p_y$, $2p_z$) participating in hybridization to give four equivalent hybrid orbitals, each of which contains 25% s character and 75% p character. These hybrid orbitals are hence referred to as the sp^3 hybrid orbitals. The carbon atom of methane was thus proposed to use four equivalent sp^3 hybrid orbitals to overlap with the 1s orbitals of four surrounding hydrogen atoms, respectively, forming four equivalent C–H bonds in an ideal tetrahedral arrangement. In the same way, the sp^3 hybridized model can be applied to molecules carrying lone pair electrons (e.g., ammonia and water, Figure 1.6), and the outcomes are consistent with the predictions of the VSEPR theory.

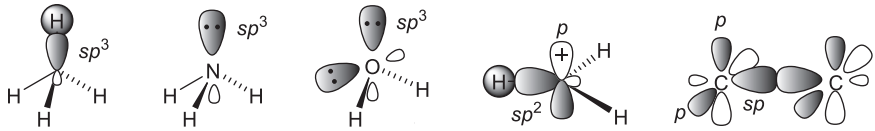

Methane	Ammonia	Water	Methyl cation	Ethyne
CH_4	NH_3	H_2O	CH_3^+	HC≡CH

Figure 1.6 Hybrid orbitals in various molecular species.

Molecular species involving unsaturated structures can be rationalized by other hybridization states. For instance, the structure of methyl cation (CH_3^+) contains three equivalent C–H bonds formed through the overlaps of three sp^2 hybrid orbitals of carbon and three 1s orbitals of hydrogen. The $2p_z$ orbital of methyl cation does not participate in the hybridization and remains empty. This orbital picture well accounts for the electron deficiency of the methyl cation. In the molecule of ethyne (HC≡CH), the carbon–carbon triple bond constitutes a σ bond (overlap of two sp hybrid orbitals of carbon) and two sets of π bonds perpendicularly oriented toward each other. Each of the π bonds is formed by overlapping two unhybridized 2p orbitals of carbon in a shoulder-by-shoulder manner. Like the Lewis structures and VSEPR theory, the hybridization-derived σ/π model also offers a convenient tool to rationalize the geometry and bonding properties of a wide range of organic compounds.

It is worth noting that hybridization is only a theoretical model to account for certain experimentally observed outcomes (e.g., bond lengths, bond angles). By no means it should be treated as a fact or experimental observable. Take methane as an example, the hybridization model predicts that the four valence electrons of carbon are located in four equivalent C–H bonds, therefore these electrons should be of the same energy. Photoelectron spectroscopic analysis indicates that the four valence electrons of carbon in methane show different binding energies (12.7 eV and 23.0 eV), which contradict the hybridization model. Clearly, the hybridization model is flawed and fails to explain the electronic energies in this case. Nevertheless, the concept of hybridization is very useful in understanding certain aspects of molecular properties, and hence it is still widely used by chemists today.

Since the hybridization theory is based on a purely mathematic treatment of atomic orbitals, the hybridization states can be various in addition to the commonly seen sp^3, sp^2, and sp types. Hybridization state can be correlated to the interorbital angle (θ) as depicted in Figure 1.7A. Herein, a hybridization index (λ) can be derived from a known interorbital angle, and the hybridization state of an orbital is expressed by sp^n, where $n = \lambda^2$. Following this method, the number n can be either an integer or a real number, depending on the value of θ. This treatment leads to the so-called **variable hybridization theory**, which can be more flexibly applied to strained molecular systems where internuclear bond

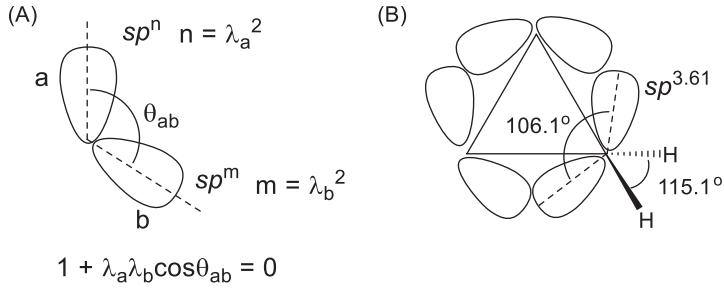

Figure 1.7 (A) Calculation of hybridization index (λ). (B) Description of the bonding properties of cyclopropane using the variable hybridization model.

angles significantly deviate from the ideal values. For example, the molecule of cyclopropane adopts a triangular shape, in which the C–C–C bond angle is 60°. This bond angle reflects the angle between the two lines crossing the positions of carbon nuclei, referred to as the **internuclear bond angle**. The angle between the two orbital lobes as depicted in Figure 1.7A is called **interorbital bond angle** (θ_{ab}), which can be obtained from the equation, $1 + \lambda_a\lambda_b\cos\theta = 0$, where λ_a and λ_b are the hybridization indexes of orbital lobes a and b. In the molecule of cyclopropane, the H–C–H bond angle was experimentally determined as 115.1°. According to the variable hybridization theory, each carbon atom of cyclopropane uses two $sp^{2.39}$ hybrid orbitals to form two equivalent C–H bonds. This will leave the carbon atom two $sp^{3.61}$ hybrid orbitals for the formation of two C–C bonds. The interorbital angle of the C–C–C bond can therefore be calculated as 106.1° using the above equation. This interorbital angle is much greater than the internuclear C–C–C bond angle, pointing to a curved shape of the C–C bond (also known as the banana bond or tau bond). The curved or bent C–C bonds of cyclopropane thus result in a large strain energy of 27.6 kcal mol^{-1}. Also, these C–C bonds show a high degree of π-bond (alkene-like) character.

In addition to molecular geometry, the hybridization state can also be used to interpret other chemical properties. For example, the relative acidity of the C–H groups in alkanes, alkenes, and terminal alkynes shows a decreasing order with increasing degree of unsaturation. A saturated alkane molecule has a pK_a value more than 60. For an alkene molecule, the pK_a value is decreased to about 43, while for a terminal alkyne the pK_a is considerably lowered to 25. The dramatically changed C–H acidity can be correlated to the hybridization states of different carbons. In a second-row atom the 2s orbital stabilizes the valence electrons much better than the 2p orbital does. Increasing the s character in a hybrid orbital should result in stronger electron attraction (i.e., enhanced electronegativity). For this reason, the degree of polarization of a C–H bond increases with increasing s character in the hybrid orbital that forms the bond. As such, the C–H acidity follows a decreasing trend of alkyne (sp) > alkene (sp^2) > alkane (sp^3).

1.3.2 Delocalized Covalent Bonds, Conjugation, and Resonance Theory

Early studies of the dihydrogen molecule using the VB theory showed that the two bonding electrons are allowed to exchange their positions with respect to the two H nuclei, which can be expressed by two wavefunctions (Φ_a and Φ_b). Heisenberg proposed that electrons are indistinguishable particles. So, the two wavefunctions can be linearly combined in two different ways ($\Phi_a + \Phi_b$) and ($\Phi_a - \Phi_b$), leading to a splitting of energy between them. Heisenberg called this term **resonance**, which was coined based on a classical analogy of two oscillators that resonate at the same frequency.

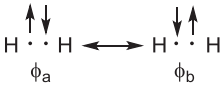

The concept of resonance [10] is useful for interpreting the electron distribution of π-conjugated molecular systems, where bonding electrons are delocalized. For example, the molecule of benzene can be described by two equivalent Lewis structures of cyclohexatriene (Kekulé structure) shown in Figure 1.8. Note that a double-headed arrow is used in resonance scheme drawing to indicate a relationship of resonance. Each of the Lewis structures is called a **resonance contributor** and it reflects partial properties of the molecule. The overall structure of a molecule can be treated as a *hybrid* of its resonance contributors.

The resonance scheme offers an intuitive tool to explain the bonding properties and charge distributions in a delocalized system. Taking the allyl cation as an example (Figure 1.8), the positive charge is shown at the two terminal allyl carbons, respectively, in the resonance scheme. Since the two resonance contributors of allyl cation are equivalent, the two terminal carbon atoms are predicted to hold an equal amount of positive charge and the two C–C bonds show an equal bond distance and bond order. In a similar way, the electronic and bonding properties of an allyl anion can be rationalized.

It is important to know that the Lewis structures drawn in a resonance scheme represent various characteristics of the same molecular species, and they should not be confused with separate chemical species in equilibrium. From the quantum

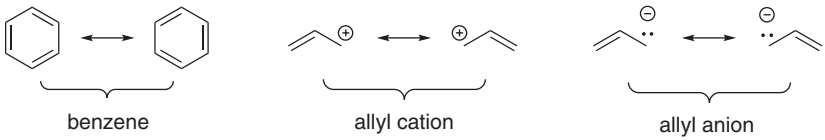

Figure 1.8 Resonance schemes of π-conjugated molecular systems.

chemical perspective, a resonance contributor is presented as a wavefunction. A linear combination of these resonance contributors (wavefunctions) describes the wavefunction of the molecule. In practice, the molecule can be understood as a resonance hybrid of its various resonance forms. The resonance contributors of a molecule therefore differ only in the assignment of electrons, but the nuclear positions shall remain unchanged. Resonance contributors can be of different significance. The contribution is weighted according to the stability of the Lewis structure. The more stable the Lewis structure, the greater the contribution it makes. A stable Lewis structure should meet the following requirements: (i) maximum number of bonds, (ii) minimum separation of opposite charges, and (iii) showing charge distribution consistent with relative electronegativity.

1.3.3 Aromaticity and Hückel Molecular Orbital (HMO) Theory

Benzene and benzene-like molecules exhibit the property called **aromaticity** [11]. Originally, aromaticity was associated with the unusual reactivity of benzene toward substitution rather than addition reactions. As described by its resonance scheme, benzene can be represented by two equivalent Kekulé structures. Structurally, benzene takes a perfect hexagon shape in which all the C–C bonds possess the same bond strength and length. Energetically, benzene is more stable than that of a non-delocalized hypothetical cyclohexatriene by about 36 kcal mol^{-1}. The extra stabilization comes from a cyclic resonance energy of benzene due to aromaticity. In the common practice, aromaticity can be described by the **Hückel's rule** as follows. Aromatic compounds usually feature a planar cyclic hydrocarbon structure that is fully π-conjugated. The π-electrons carried by the **aromatic** ring should be a (4n + 2) number, where n is 0 or any integer. If the number of π-electrons is 4n, the system is called **anti-aromatic**. Following this rule, planar cyclic structures with (4n + 2) π-electrons in Figure 1.9 can be categorized as being aromatic. The planar cyclic structures with 4n π-electrons are anti-aromatic and therefore cannot exist as stable species. If a molecular structure significantly deviates from planarity, it is viewed as **non-aromatic** due to the disruption of cyclic π-conjugation over a non-planar ring. For example, if cyclooctatetraene adopts a planar conformation, it would exhibit anti-aromaticity. However, the eight-membered ring of cyclooctane favors a tub-shaped conformation due to the angle strain in the eight-member ring (see Figure 1.9). So, in the stable conformation of cyclooctatetraene, the p orbitals of two adjacent C=C bonds are in a nearly perpendicular orientation. This leads to poor orbital overlap and hence the π-electrons are localized in each C=C bond.

Theoretically, the Hückel's rule was derived from the **Hückel molecular orbital** (HMO) theory [12], which is a simplified but very efficient method to elucidate the molecular orbital properties for π-conjugated systems. In the HMO method, only the interactions of adjacent p atomic orbitals are considered. The π

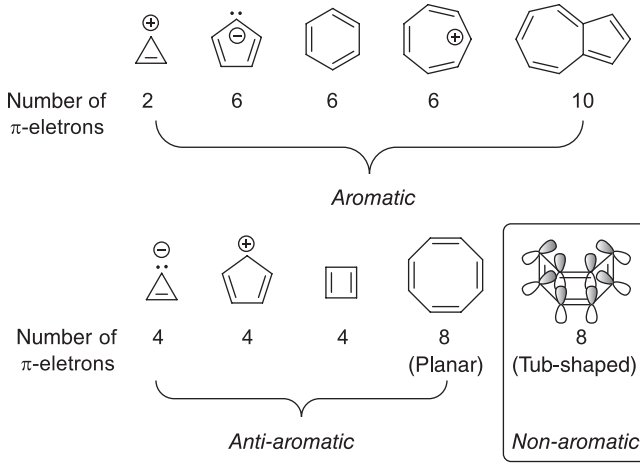

Figure 1.9 Typical hydrocarbon rings showing aromaticity, anti-aromaticity, and non-aromaticity.

MOs resulting from the overlap of a set of p orbitals can be calculated by solving a secular equation. For a linear polyene, the energy levels of HMOs are given by the equation, $E_i = \alpha + m_i\beta$, where α is called the Coulomb integral, β is called the resonance integral, $m_i = 2\cos(j\pi/(n+1))$, and j is the orbital number ($j = 1, 2, 3, ..., n$). For a monocyclic π-conjugated system, the HMO energies are given by the equation, $E_i = \alpha + m_i\beta$, where $m_i = 2\cos(j\pi/n)$. A device called the **Frost circle** can assist to conveniently obtain the MO energies as illustrated in Figure 1.10. First, a perfect polygon is inscribed in a circle with one vertex down. The radius of the circle is 2β, and the level at the center of the circle is set as α. The HMO energy levels are at the positions of the vertexes of the polygon, which can be determined geometrically.

The HMO theory allows the stabilization energy of an aromatic ring such as benzene to be estimated by comparing its total π-electron energy with that of 1,3,5-hexatriene. As shown in Figure 1.11, the two π-conjugated systems have the same number of C=C bonds; however, the lack of cyclic π-conjugation (i.e., aromaticity) makes 1,3,5-hexatriene less stabilized than benzene by 1.012β (ca. 22 kcal mol^{-1}).

Apart from the Hückel's rule, aromaticity can also be quantitatively assessed through methods based on structural, energy, reactivity, and magnetic criteria. The following describes several representative methods that have been popularly used in recent years. Structurally, aromaticity leads to **bond length alternation** (BLA). In this respect, **harmonic oscillator for aromaticity** (HOMA) is popularly used as an index of aromaticity [13]. HOMA can be calculated by the following equation:

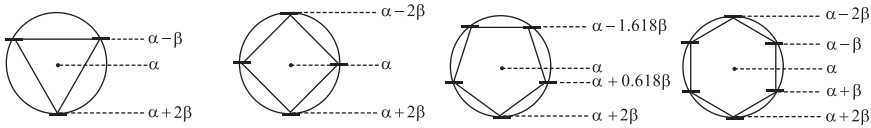

Figure 1.10 Energy level diagrams for monocyclic π-conjugated systems generated with the aid of the Frost circle.

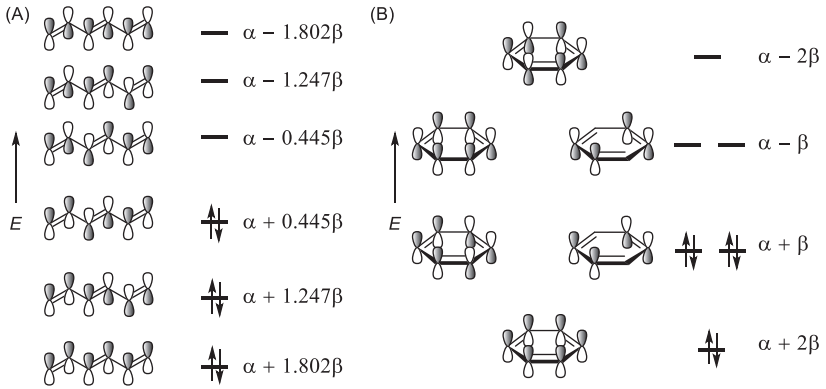

Figure 1.11 HMO plots for 1,3,5-hexatriene (A) and benzene (B).

$$\mathrm{HOMA} = 1 - [a(R_{opt} - R_{av})^2 + a/n\sum(R_{av} - R_i)^2]$$

where R_{av} is the average bond length, R_{opt} is the optimum bond length, R_i is an individual bond length, n is the number of bonds, and α is an empirical constant that makes the HOMA of a localized non-aromatic structure *zero*. Energetically, aromaticity can be assessed by an index called **aromatic stabilization energy** (ASE), which is calculated based on a carefully selected thermodynamic cycle for a hypothetical **homodesmotic reaction** that involves breaking the π-conjugation in the ring of interest. A homodesmotic reaction belongs to the class of so-called **isodesmic reactions**, in which reactants and products contain equal numbers of atoms in corresponding states of hybridization. Moreover, there is matching of the carbon–hydrogen bonds in terms of the number of hydrogen atoms joined to the individual carbon atoms. They serve as useful tools for studying the energy and thermochemistry of molecules.

According to the HMO theory, aromatic systems tend to possess a relatively large energy gap between the **highest occupied molecular orbital** (HOMO) and **lowest unoccupied molecular orbital** (LUMO). According to the Koopmans theorem, the HOMO-LUMO gap ($\Delta E_{\mathrm{HOMO\text{-}LUMO}}$) is equal to the **hardness** (η) of the molecule, which is a quantity introduced by Pearsons in his well-known

hard/soft acids and bases (**HSAB**) principle [14, 15]. The relatively large $\Delta E_{\text{HOMO-LUMO}}$ of an aromatic compound (e.g., benzene) is consistent with its reduced reactivity toward electrophiles. In contrast, anti-aromatic compounds have small HOMO-LUMO gaps and therefore are reactive and relatively unstable.

Nuclear magnetic resonance (NMR) spectroscopy provides an effective tool to assess aromaticity, since the delocalized π-electrons in an aromatic compound tend to form a diamagnetic ring current when subjected to the influence of an external magnetic field [16]. The ring current strongly affects the ^{1}H and ^{13}C chemical shifts. Schleyer and co-workers devised a popular method to correlate chemical shift (δ) and aromaticity, called the **nucleus independent chemical shift** (NICS) [17]. It evaluates aromaticity based on the magnetic shielding at the center of a ring of interest calculated using *ab initio* or density functional theory (DFT) methods. When calculating NICS values, dummy atoms are placed at the centroid of an aromatic ring and various positions above it. A dummy atom is a hypothetic atom that does not possess any electrons or a nucleus. It is therefore only used to define a coordinate for probing the chemical shielding at its location in quantum mechanics calculations. The negative value of the calculated chemical shift (δ) of the dummy atom placed at the ring center gives the NICS(0) (Figure 1.12). A ring that shows a large negative NICS(0) value is considered as aromatic, while a large positive value indicates anti-aromaticity. For example, benzene and benzenoid hydrocarbons show NICS(0) values of −9 to −10 ppm. Anti-aromatic cyclobutadiene features a NICS(0) value of +27.6 ppm. In addition to the ring center, the dummy atom can also be placed at a position 1.0 Å vertically above the center of the ring to obtain the NICS(1.0) value. The advantage of using NICS(1.0) as a criterion for aromaticity is that the ring current usually maximizes at this position and the influences of other structural factors are relatively small.

Aromaticity can be found in cyclic π-conjugated systems, where the π-conjugation of the ring is interrupted by one or more than one saturated linkage(s) but orbital overlap still occurs due to the geometry of the molecule. Such structures are deemed to possess **homoaromaticity** [18]. Furthermore, the systems can be defined as mono-, bis-, and tris-homoaromatic according to the number of interruptions to

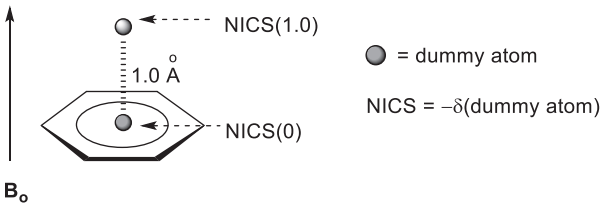

Figure 1.12 Calculations of NICS(0) and NICS(1.0) for benzene with the aid of dummy atoms (shaded circles). B_0 is the external magnetic field and δ is the calculated chemical shift (in ppm).

π-delocalization. Figure 1.13 lists a selection of mono-homoaromatic cationic and anionic cyclic π-systems, where (4n + 2) π-electrons are delocalized through a loop of overlapped p orbitals. These homoaromatic ions have been found to show enhanced stability; however, the stabilizing effects are not as strong as those in the aromatic systems.

The delocalization of a charge in the cationic and anionic systems in Figure 1.13 is a significant factor enabling them to exhibit homoaromaticity. Examples of neutral homoaromatic systems have also been proposed and studied, but the homoaromaticity of many of such systems has been determined to be either very weak or in dispute. For example, Figure 1.14 lists a series of neutral systems showing mono-, bis-, and tris-homoaromaticity. Cycloheptatriene (Figure 1.14A) has a saturated CH_2 group linking the two ends of a conjugated triene. Partial π-orbital overlap between the two ends was proposed to form a benzene-like delocalization pattern. It has been regarded as a marginally homoaromatic system. Semibullvalene (Figure 1.14B) can undergo a degenerate Cope rearrangement through a low-lying

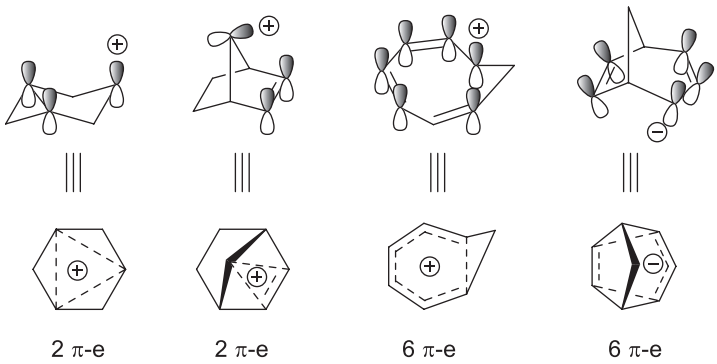

Figure 1.13 Examples of cationic and anionic homoaromatic systems.

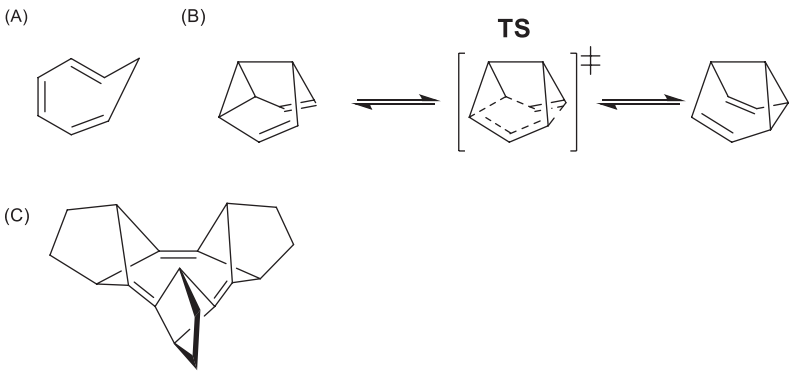

Figure 1.14 Examples of neutral homoaromatic systems.

transition state ($\Delta G^{\neq} = 6.2$ kcal mol^{-1}). In this transition state, four π-electrons and two σ-electrons are fully delocalized, exhibiting a bis-homoaromaticity. Stahl et al. investigated a strained cyclic triene system (Figure 1.14C) through systematic computational analyses and convincingly demonstrated it as a neutral tris-homoaromatic system [19].

Fully π-conjugated cyclic systems may feature a Möbius topology in terms of the arrangement of p-orbital overlap to show aromaticity, which is known as the **Möbius aromaticity** [20]. A Möbius strip can be constructed from a rectangular strip by first giving one of the ends a one-half twist and then affixing the two ends together. This type of strip exhibits interesting properties, such as having only one side and remaining in one piece when split down the middle. Figure 1.15 depicts the contrast between typical planar cyclic π-conjugation (i.e., Hückel system) and a Möbius π-system. In contrast to the Hückel system, a Möbius ring structure carrying 4n π-electrons is considered as aromatic, while (4n + 2) π-electrons lead to anti-aromaticity. Möbius aromatic compounds do not naturally exist; however, synthetic chemists have successfully constructed certain twisted annulenes and porphyrins that show Möbius aromaticity [21–23].

1.3.4 Hyperconjugation and Orbital Interactions

Resonance theory explains the properties of electrons delocalizing among π-bonds and/or non-bonding p orbitals that show a significant degree of overlap. Electron pairs of σ-bonds are not considered migratable under the assumption that they do not overlap significantly with π and p orbitals. Therefore, σ-bonds are not allowed to be broken in resonance scheme drawing. Nevertheless, electron delocalization between a σ–bond and its neighboring π/p orbitals can still occur, resulting in a significant effect on chemical stability and reactivity. Such effect is known as the **hyperconjugation effect** [24], which can be conveniently explained by the **orbital interaction theory** [25–27]. Figure 1.16 illustrates the stabilizing effect on the ethyl cation and propene due to hyperconjugation. In the ethyl cation, the C–H σ-bond overlaps with the empty p orbital of the carbocation to some extent,

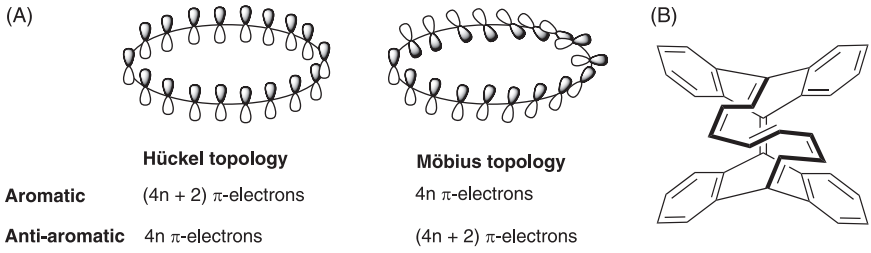

Figure 1.15 (A) Illustrations of π-systems showing Hückel and Möbius topologies. (B) A stable Möbius annulene.

although the overlap is not as large as the overlap of two p orbitals aligned in parallel. The delocalization of C–H bonding electrons to the p orbital can be illustrated by using a resonance scheme, which reveals that the hydrogen atom of the C–H has a partial cation character and the C–C bond has a partial double bond character. Qualitative molecular orbital drawings can also assist in understanding the stabilizing effect of hyperconjugation. According to the molecular orbital theory, the mixing of two overlapping orbitals results in two molecular orbitals. The low-lying orbital is called a **bonding orbital**, and the high-lying orbital is called an **antibonding orbital**. As shown in Figure 1.16, the interaction of the C–H bond and the adjacent empty p orbital leads to an electron pair populated in the low-lying bonding orbital, while the high-lying antibonding orbital remains unoccupied. Overall, the system gains stability from the hyperconjugation effect. Similarly, the stabilizing effect of an alkyl group substituted on an alkene unit can be explained by hyperconjugation. Take propene as an example, hyperconjugation occurs between the methyl C–H bond and the antibonding orbital of the C=C double bond. The resonance scheme drawing reveals that one of the C=C carbon atoms possesses a partial carbanion character, indicating that the π-electron density is enhanced by alkyl substitution.

Stabilizing effects similar to hyperconjugation can be found in systems where a donor orbital effectively interacts with an acceptor orbital. A donor orbital can be an electron-rich – bond or a non-bonding orbital occupied by an electron lone pair. An acceptor orbital is usually an empty p orbital, the antibonding orbital of a polar C–X bond (σ^*), or a low-lying antibonding π^* orbital. For example, the C–H bond (donor) in 1,2-difluoroethane interacts with the antibonding orbital of the adjacent C–F bond (acceptor) when they are aligned antiparallel to gain stabilization (Figure 1.17A). As such, the 1,2-difluoroethane molecule prefers a conformation where the two fluoro groups are gauched, known as the **gauche effect**. When a filled p or π orbital interacts with an adjacent σ^* orbital, stabilization is gained. This is generally referred to as the **negative hyperconjugation** [27, 28]. For example, the methoxy group of 2-methoxytetrahydropyran prefers to take the axial position rather than the equatorial position (Figure 1.17B). This phenomenon is known as the **anomeric effect**, the origin of which can be rationalized by the maximum orbital interaction between one of the oxygen lone pair orbitals and the vertically oriented C–O antibonding orbital (σ^*_{C-O}) in this conformer. Negative hyperconjugation can lead to significantly altered spectroscopic properties. For example, the stretching of the C–H bond of an aldehyde occurs at 2700–2800 cm^{-1}, which is much lower than the vibrational frequency of a typical sp^2 C–H bond (around 3050 cm^{-1}). This result can be explained by the fact that the one of the oxygen lone pair orbitals is aligned antiparallel to the C–H bond, enhancing the interaction between the oxygen lone pair orbital and the C–H antibonding orbital. As such, the C–H bond of an aldehyde is lengthened and weakened. This effect can be illustrated by the negative hyperconjugation scheme in Figure 1.17C.

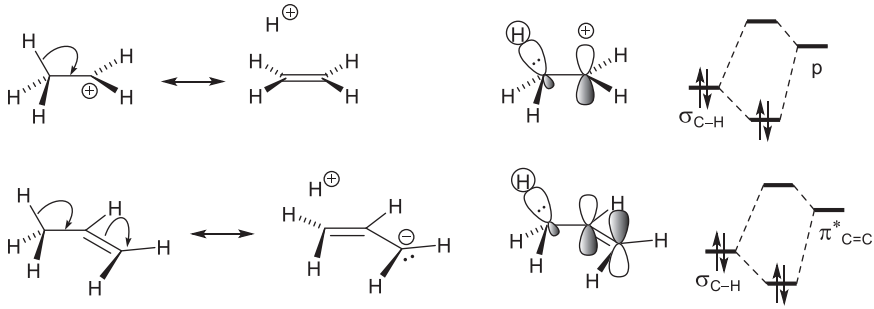

Figure 1.16 Hyperconjugation effects taking place in ethyl cation and propene.

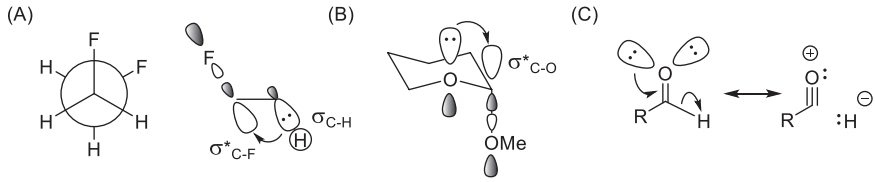

Figure 1.17 Examples of hyperconjugation interactions in organic structures.

1.4 Non-Covalent Interactions and Supramolecular Chemistry

Many organic nanostructures and materials are assembled at the supramolecular level, utilizing various non-covalent interactions as the key forces to influence and control the structural and electronic properties as well as material functions of interest. **Supramolecular chemistry**, as defined by Jean-Marie Lehn, deals with the "chemistry beyond molecules." The original studies of supramolecular chemistry began with the development of guest–host chemistry, mainly focusing on understanding the non-covalent interactions between a host and a guest molecule. Nowadays this field has been vastly expanded to cover many disciplines. Non-covalent interactions arise from various attractive and repulsive forces between molecules and ions. They can be generally classified into the following types.

1.4.1 Electrostatic Interactions Involving Ions and Dipoles

Ions of opposite charges show strong electrostatic (i.e., Coulombic) attraction. The ion–ion interactions are usually of comparable strength to covalent bonding, leading to the formation of ionic solids, such as various inorganic salts. Some specially designed organic cations can attract anions to form supramolecular assemblies, in which the ion–ion attraction plays an important role. For example, the

organic trication derived from 1,3,5-tris(bromomethyl)-2,4,6-trimethylbenzene and (1,4-diazabicyclo[2.2.2]octane) (DABCO) can form a crystalline material through ion–ion interactions with ferricyanide anion (Figure 1.18) [29].

An ion can interact with a molecule that possesses a permanent dipole. Such an interaction is called an **ion–dipole interaction**, the strength of which is dependent on the geometric parameters for the arrangement of the ion and the dipole. As shown in Figure 1.19A, the dipole moment (μ) can be determined by the equation, $\mu = q_1 \times r$, where q_1 is the amount of charge accumulated at the end of dipole and r is the distance of charge separation. The potential energy (E) for the dipole interacting with an ion carrying a charge of q_2 can thus be determined using the following equation

$$E = \frac{\mu q_2 cos\theta}{4\pi\varepsilon\varepsilon_0 d^2} \tag{1.1}$$

where θ and d are the angle and distance of the ion with respect to the dipole (see Figure 1.19A), ε is the relative permittivity (or dielectric constant) of the medium, and ε_0 is the vacuum permittivity.

Ion–dipole interaction plays a critical role in the solvation of cations by strongly dipolar solvents, such as water, DMF, and DMSO. As illustrated in Figure 1.19B,

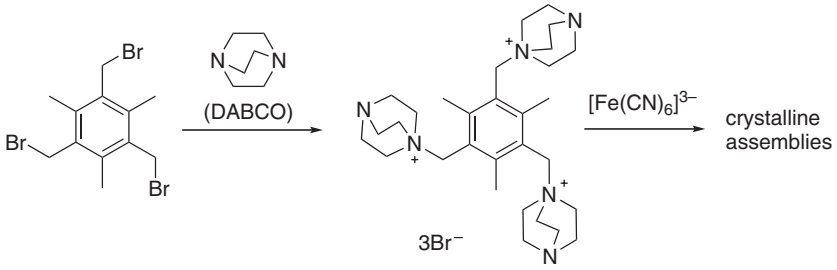

Figure 1.18 A designed organic trication for self-assembly with ferricyanide.

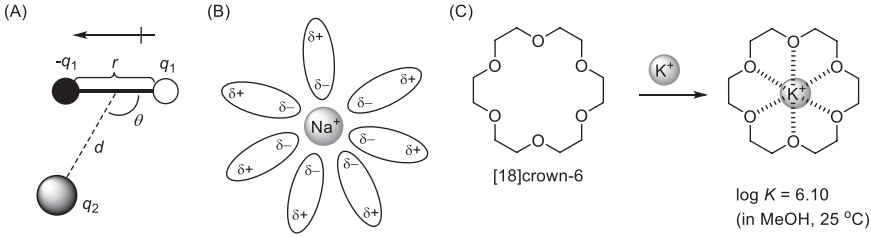

Figure 1.19 (A) Parameters of an ion–dipole interaction. (B) Favored arrangement of dipolar solvent molecules surrounding a sodium cation. (C) Complexation of [18]crown-6 with a potassium cation.

polar solvent molecules can form a solvation shell in which the partially negatively charged ends of the solvent molecules are drawn close to the cation through ion–dipole interactions. For cations with the same charge but different sizes, the ion–dipole interaction energy increases with decreasing ion size. This is because the smaller radius of the ion, the higher the charge density per unit area it affords and hence the resulting Columbic interaction. Cyclic and cage-like organic molecules with preorganized polar bonds can act as good supramolecular hosts for various cations. A well-known example is the class of crown ether molecules. For example, [18]crown-6 (IUPAC name 1,4,7,10,13,16-hexaoxacyclooctadecane) can form a stable 1:1 complex with a potassium ion. In this complex, all the polar C–O bonds are favorably arranged to enhance the ion–dipole attractions (Figure 1.19C).

Similar to an ion–dipole interaction, two dipoles in close proximity can give rise to attractive or repulsive forces (**dipole–dipole interaction**) depending on their relative orientations. As shown in Figure 1.20A, when two dipoles are closely positioned, their ends with opposite charges would induce Coulombic attraction, while the ends whose charges have the same sign repel each other. The potential energy of a dipole–dipole interaction can be calculated following the scheme and equation illustrated in Figure 1.20B. Since the energy of dipole–dipole interaction is inversely proportional to the cube of their distance (d^3) apart, the strength of a dipole–dipole force is very sensitive to distance. Compared with ion–dipole interactions, the strength of dipole–dipole interactions is weaker and more dependent on direction. Usually, polar molecules prefer to be aligned in such a way that the positively charged pole closely approaches the negatively charged pole (see Figure 1.20C) to give the strongest possible interaction. For molecules with resonance-stabilized charge separation, dipole–dipole interactions among them are further enhanced. For example, amides show strong resonance effects in which the lone

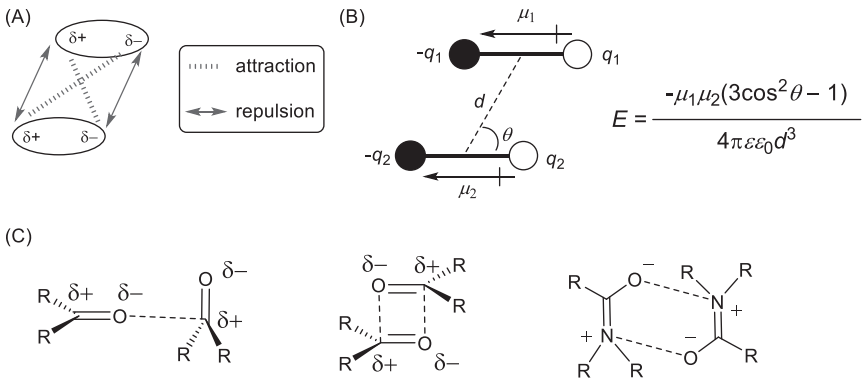

Figure 1.20 (A) Electrostatic attraction and repulsion in a dipole–dipole interaction. (B) Calculations of dipole–dipole interaction energy. (C) Dipole–dipole interactions among ketone and amide molecules.

pair electrons of the N atom are delocalized with the antibonding orbital of the adjacent C=O π-bond. As such, an amide molecule would show a large permanent dipole with enhanced charges on the N and O ends, which in turn strengthens the pairing of two oppositely aligned amide molecules through dipole–dipole interactions (Figure 1.20C). The strong intermolecular attractions thus make amides exhibit much higher boiling and melting points than other carboxylic acid derivatives with similar molecular sizes.

Furthermore, it is worth noting that when two dipoles are aligned at an angle (θ) equal to 54.7°, the term ($3\cos^2\theta-1$) turns into zero and the dipole–dipole interaction vanishes. This angle is known as the **magic angle**, which is used in a special technique for solid-state NMR spectroscopy, namely **magic angle spinning** (MAS), to eliminate the line broadening effect due to nuclear dipolar interactions.

1.4.2 Hydrogen Bonding Interactions

Hydrogen bonding is a very important type of binding force, specifically referred to the attractive interaction of a hydrogen atom with an electronegative atom [30]. Usually, a hydrogen bond exists in the form of D–H···A, where D–H is a **hydrogen bond donor** and A is a **hydrogen bond acceptor**. The D unit in D–H is usually an electronegative atom such as N, O, or S, so that the hydrogen atom connected to it exhibits a partial positive charge and becomes somewhat acidic. The A group often bears a relatively high-energy electron lone pair(s) and possesses a partial negative charge, making it attractive to the acidic proton of D–H through Coulombic interaction. In this sense, hydrogen bonding can be viewed as a special type of dipole–dipole interaction or acid–base interaction.

Hydrogen bonding ubiquitously exists in supramolecular chemistry and is regarded as the "master key to molecular recognition." Normal hydrogen bonds show bond strengths ranging from about 1 to 14 kcal mol^{-1}. The strength of a hydrogen bond is associated with the electronegativity of the two counterparts, D in D–H and A. For a hydrogen bond donor (D–H), its hydrogen bond donating ability increases with increasing electronegativity of the D unit. So is the hydrogen bond accepting ability for an A group. When a hydrogen bond involves an ion (e.g., hydronium ion or fluoride anion), the hydrogen bond strength can be considerably enhanced (see Figure 1.21).

Hydrogen-bonded systems can adopt different geometries as summarized in Figure 1.22. These geometries result from direct interactions of hydrogen bond donor and acceptor groups, and they are referred to as the **primary hydrogen bonding interactions**. In a D–H···A interaction, the hydrogen bond angle can be linear or deviated from linearity (bent), depending on the orientation of the lone pair electrons on the A group. For example, when the A group involves only one electron lone pair (e.g., amino, cyano), a colinear arrangement of D–H···A is expected. When there are more than one electron lone pairs on the A group

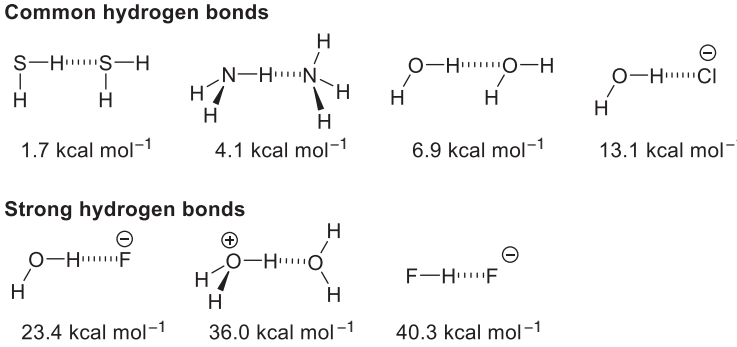

Figure 1.21 Examples of hydrogen-bonding interactions and hydrogen bond strengths.

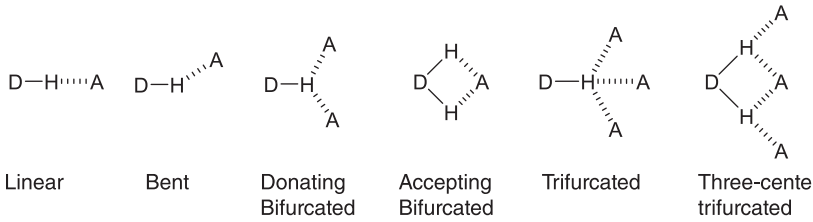

Figure 1.22 Geometries of primary hydrogen bonding interactions.

(e.g., hydroxy, carbonyl), the hydrogen-bonded geometry is consistent with the electron lone pair orientations, which can be reasonably predicted by the VSEPR theory. Usually, the linear hydrogen-bonding motifs show stronger binding forces than the bent ones.

When hydrogen bonds are formed between two or more molecules of the same type, they are called **homo-intermolecular hydrogen bonds**. For example, imidazole molecules can form a linear network through homo-intermolecular hydrogen bonds (Figure 1.23A). A carboxylic acid and an amide (primary and secondary) can dimerize through homo-intermolecular double hydrogen bonds (Figure 1.23A). Hydrogen bonding interactions between molecules of different types give the **hetero-intermolecular hydrogen bonds** (Figure 1.23B). A hydrogen bond can also occur within the same molecule, known as an **intramolecular hydrogen bond** (Figure 1.23C). Usually, an intramolecular hydrogen bond favors the formation of a stable six-member ring motif. On the other hand, intramolecular hydrogen-bonded five-, seven-, and eight-member rings also exist.

When hydrogen bonding interactions occur between arrays of hydrogen bond donors and acceptors which are in close proximity, **secondary hydrogen bonding interactions** also play a notable role in the stability of the hydrogen-bonded assemblies. Figure 1.24 exemplifies three hydrogen-bonded molecular

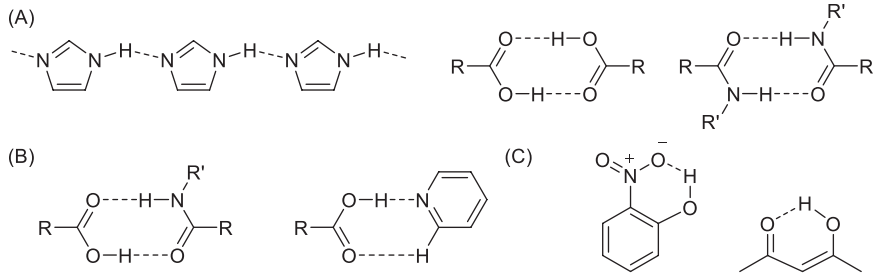

Figure 1.23 Examples of (A) homo-intermolecular, (B) hetero-intermolecular, and (C) intramolecular hydrogen bonds.

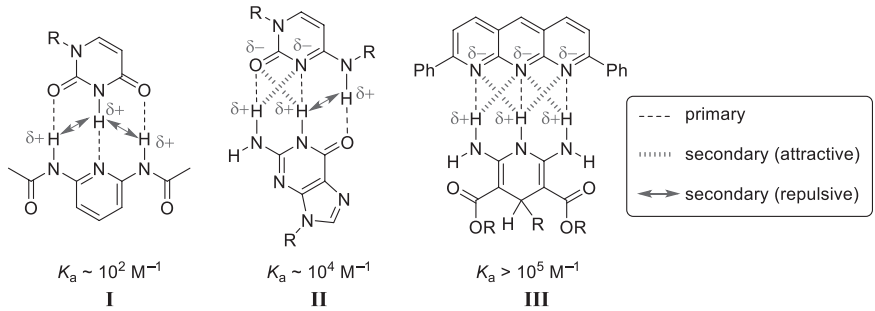

Figure 1.24 Hydrogen-bonded supramolecular assemblies with varied degrees of secondary hydrogen bonding interactions.

pairs, each of which consists of three hydrogen bonds. The hydrogen bond donor (D) and acceptor (A) groups in these structures are in different arrangements. The first hydrogen-bonded assembly **I** contain two counterparts, which are in the DAD and ADA motif, respectively. The secondary interactions as illustrated afford only repulsive forces. In assembly **II**, the motifs are changed to DDA and AAD. As such, the secondary interactions give two attractive forces and one repulsive force. The third structure **III** is a DDD and AAA assembly, where all the secondary interactions give attractive forces. The differences in their secondary hydrogen bonding interactions make these three hydrogen-bonded assemblies show very different association constants (K_a). Of these structures, only **III** exhibits all attractive interactions, while **I** and **II** show repulsive secondary interactions to varied extents. As a result, **III** possesses the highest stability among them.

The formation and properties of hydrogen bonds can be investigated by a variety of experimental methods, such as vibrational and NMR spectroscopic analyses. For example, the hydrogen bonding interaction in a D–H···A system would lengthen the D–H bond and give rise to new vibrational modes due to the H···A bond. In the NMR analysis, pronounced proton deshielding for the

H in D–H can be observed as a result of hydrogen bonding. Energetically, the formation of a hydrogen-bonded assembly makes the Gibbs energy of formation greater than the thermal energy of the system, which can be experimentally determined. Hydrogen bonds are directional and can strongly influence crystal packing modes. Crystallographic analysis can therefore cast a deep insight into the roles of hydrogen bonds in the solid state. Besides experimental methods, computational studies based on quantum chemical theories are of great value in characterizing and assessing hydrogen bonds. A popular theoretical method, which is often used in combination with experimental analysis, is to perform critical point analysis on the electron density topology of the molecular system based on the theory of **atoms in molecules** (AIM) proposed by Bader [31]. In 2011, a task group of International Union of Pure and Applied Chemistry (IUPAC) published an article, entitled *Definition of the hydrogen bond (IUPAC Recommendations 2011)*, which offers updated definition and criteria for the hydrogen bond [32].

1.4.3 Interactions Involving π-Systems

As discussed above, π-electrons delocalize on the skeleton of an aromatic ring, resulting in an extra stabilization attributed to aromaticity. The electronic properties of aromatic compounds would also lead to unique π-effects in their non-covalent interactions, commonly called **π-stacking** or **π–π interactions** [33–35]. In benzene, for example, high electron density is present around the central region of the benzene ring, while the six hydrogen atoms on the edges are electron deficient. Such an electron distribution pattern can be rationalized by the polar nature of benzene's sp^2 C–H bonds. A typical C–H bond in an alkane is non-polar, since the sp^3 hybridized carbon has similar electronegativity to hydrogen. The sp^2 hybridized carbons in benzene, on the other hand, are more electronegative due to their larger percentage of s character (33.3%) involved in hybridization. As a result, the C–H bonds of benzene show a significant bond dipole moment. Although the hexagon-shape of benzene makes the C–H bond dipoles cancel one another to yield a zero net molecular dipole moment, a quadrupole moment exists in benzene as illustrated in Figure 1.25. Because of this, benzene can still show electrostatic attraction to various cationic and polar species in a manner similar to ion–dipole and dipole–dipole interactions.

Figure 1.26 shows various modes of π-interactions for benzene. Since benzene has a significant quadrupole moment, it can interact with a cation through electrostatic attraction. Figure 1.26A shows the equilibrium geometry of a benzene/cation complex, known as a cation-π interaction. Herein the cation favors alignment with the center of benzene, which is the orientation that maximizes the electrostatic attraction. The equilibrium distances and binding energies for the 1:1 complexes of benzene with various cations are listed in Table 1.1. As

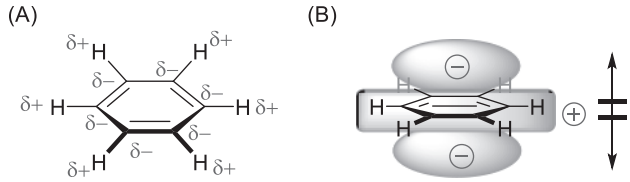

Figure 1.25 Illustrations of (A) the polar C–H bonds and (B) quadrupoles of benzene.

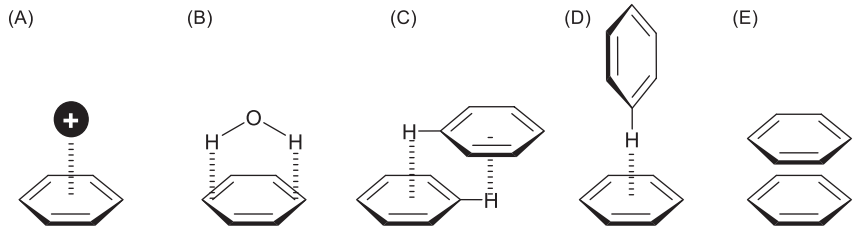

Figure 1.26 Various π-interactions of benzene. (A) cation–π interaction, (B) polar-π interaction, (C) parallel-displaced π-stacking, (D) edge-to-face π-stacking, (E) eclipsed face-to-face π-stacking.

Table 1.1 Equilibrium distances (D) and binding energies ($E_{binding}$) for 1:1 complexes of benzene with various alkali and alkaline metal cations [36].

Cation	D (Å)	$E_{binding}$ (kcal mol^{-1})
Li^+	1.85	−35.9
Na^+	2.44	−21.5
K^+	3.05	−13.1
Mg^{2+}	1.95	−111.9
Ca^{2+}	2.47	−66.7

Data calculated at the MP2/Sadlej level of theory.

can be seen, the binding strength increases with decreasing ion size and increasing charge. Besides metal cations, benzene and benzene-containing aromatic compounds can also interact with organic cations (e.g., ammonium ions) through the cation−π interaction.

Benzene can also show attractive interactions with molecules with strong permanent dipoles, which are called **polar-π interactions**. For example, the interaction energy of benzene and water was experimentally determined to be about 2.4 kcal mol^{-1}. The binding mode is depicted in Figure 1.26B, in which the two partially positively charged protons of water are in contact with the

electron-rich sp^2 carbons of benzene. In a sense, this interaction is a weak hydrogen bonding interaction. It is worth noting that benzene is a hydrophobic compound that is immiscible with water. However, the hydrophobic (water-hating) behavior is not a result of repulsive interactions between benzene and water molecules. We shall be very clear that benzene and water attract one another through polar–π interactions. The hydrophobic behavior mainly comes from an entropic origin which will be discussed in detail in Section 1.4.6.

π-Stacking can occur among molecules of benzene and benzene-like aromatic molecules. Two commonly seen stacking modes of benzene are illustrated in Figure 1.26C and D, which are called parallel-displaced (slipped) and edge-to-face (T-shaped) π–stacking, respectively. In these two stacking modes, the positively charged edge of one benzene molecule is in a close contact with the centroid region of another benzene where the negatively charge electron cloud is populated. Therefore, the parallel-displaced and edge-to-face stackings are both energetically favored. The edge-to-face stacking is energetically favored and therefore more frequently observed in crystal packing structures. The eclipsed face-to-face (sandwich) stacking of benzene (Figure 1.26E) align the regions of positive and negative electrostatic potentials, respectively. Actually, this stacking mode leads to an electrostatic repulsion and hence is disfavored. It is worth cautioning that the term "π-stacking" or "π–π interactions" would mislead one to consider that the eclipsed face-to-face is favored. So, a clear understanding of the origins of these π–π interactions is necessary before using such terms.

1.4.4 Induced-Dipole Forces

Molecules that are lacking permanent dipoles can still show attractive electrostatic interaction with a polar species or a nonpolar molecule in close proximity [37]. When subjected to an external field, a molecule will respond with changes in the distribution of its electron density, which can be described by a property called **polarizability** (α). The polarization of the electron cloud of a nonpolar molecule creates a temporary dipole moment (μ), which in turn gives electrostatic attraction toward ions or molecules nearby. Figure 1.27 illustrates three exemplar scenarios of induced-dipole formation.

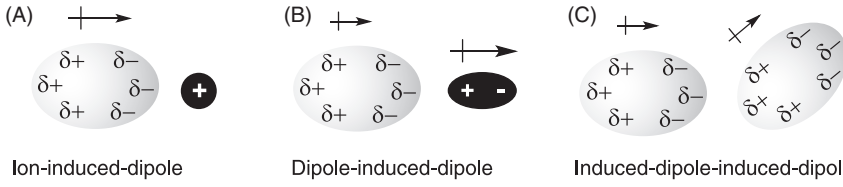

Figure 1.27 Schematic illustrations of the formation of induced-dipoles of nonpolar molecules.

Figure 1.27A depicts the ion-induced-dipole interaction, the energy of which (E) can be determined by the following equation:

$$E = \frac{-q^2\alpha}{(4\pi\varepsilon\varepsilon_0)^2 r^4} \tag{1.2}$$

where q is the charge of the cation, α is the polarizability of the molecule, and r is the distance between the centroids of the ion and the molecule. As can be seen that the interaction energy E is dependent on $1/r^4$, indicating that the attractive force would diminish very rapidly as the distance increases. Likewise, a molecule with a permanent dipole moment can polarize a nonpolar molecule when approaches it closely. The induced dipole of the nonpolar molecule aligns with the permanent dipole to give an electrostatic attraction, known as an **dipole-induced-dipole interaction** (Figure 1.27B). Compared with the ion-induced-dipole interaction, this force is even more sensitive to distance, showing a dependence on $1/r^6$.

When a nonpolar molecule is instantaneously polarized to generate a temporary dipole, it can exert the same effect on a nearby nonpolar molecular as a permanently dipolar molecule does (see Figure 1.27C). This type of force is called an **induced-dipole-induced-dipole interaction**, which has also been well known as a **London dispersion interaction**. The magnitude of such interaction is considerably small, but it plays a significant role in the intermolecular interactions in condensed liquids such as alkanes and alkenes. For example, an alkane with a linear zigzag molecular backbone shows a higher boiling point than its structural isomers that show branched molecular structures. This is because the linear alkane molecules can be more efficiently packed (due to more effective contact areas) to afford stronger intermolecular attractions.

1.4.5 Charge-Transfer Interactions

When a donor (D) and an acceptor (A) molecule are closely stacked, a fraction of electronic charge is transferred from the HOMO of the donor to the LUMO of the acceptor, resulting in an electrostatic attraction between them, called the **charge-transfer (CT) interaction**. Like hydrogen bonding, the CT interaction is a directional intermolecular force that plays an important role in supramolecular chemistry. A vast array of redox-active organic π-chromophores, mainly aromatic compounds, can form D···A complexes through CT interactions. Figure 1.28 shows a selection of organic π-donors and π-acceptors [38].

The strength of D···A complexation is dependent on several of parameters, including the donating and accepting ability of the D and A molecules, steric crowding in their structures, the shape complementarity of their π-surfaces, and

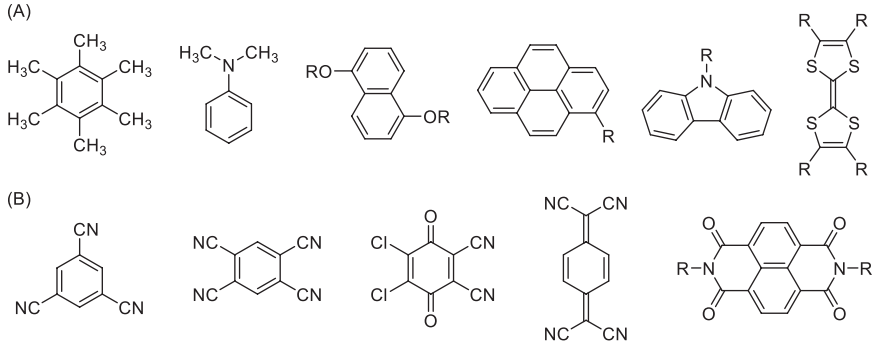

Figure 1.28 Examples of (A) organic π-donors and (B) organic π-acceptors.

the solvent effects. The binding affinity between neutral π-donor and π-acceptor molecules in the solution phase is usually not very strong. For example, hexamethylbenzene (HMB) is an organic π-donor that can form a 1:1 complex with electron-deficient 1,3,5-trinitrobenzene (TNB), affording an association constant (K_a) of 15.5 ± 0.4 M^{-1} in cyclohexane at 20 °C. When the solvent is switched to chloroform, the K_a is attenuated to 0.76 ± 0.05 M^{-1}. Tetrathiafulvalene (TTF) and its derivatives are an important class of organic π-donors. Their excellent electron-donating ability is due to their aromaticity-stabilized oxidized states. As shown in Figure 1.29A, a TTF molecule can sequentially release two electrons to yield a radical cation and dication, respectively. In each of the cationic products, the five-membered dithiolium ring features a 6 π-electron cyclic conjugation pattern. According to the Hückel's rule, the dithiolium ring is aromatic. The aromaticity-stabilized oxidized products of TTF enable it to release electrons at relatively low potentials. TTF can efficiently complex with cyclobis(paraquat-*p*-phenylene) (**CBPQT**$^{4+}$) with a large association constant in solution (Figure 1.29B). Such CT interactions have been extensively used in the formation of interlocked compounds such as rotaxanes and catenanes, to which Sir J. Fraser Stoddart has made tremendous contributions, leading him to winning the 2016 Nobel Prize in Chemistry.

In the solid state, TTF and its derivatives can form CT salts with strong π-acceptors, such as 7,7,8,8-tetracyano-*p*-quinodimethane (TCNQ). Figure 1.30 illustrates the solid-state structure of a CT salt of dibenzo-tetrathiafulvalene (DB-TTF) and TCNQ, in which the D and A molecules are organized to form [···D–A-D–A···] alternating stacks through CT interactions [39]. TTF-based CT salts show intriguing metallic and semiconducting behavior useful for organic electronic applications. Besides crystalline solids, CT interactions can also be utilized as a major driving force to generate functional materials such as organogels, foldamers, and liquid crystals.

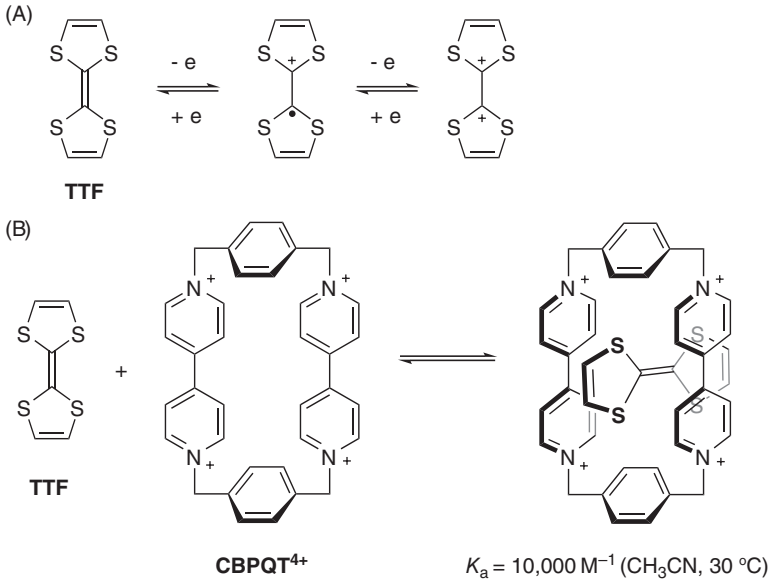

Figure 1.29 (A) Stepwise oxidation of tetrathiafulvalene (TTF). (B) 1:1 Complexation of TTF and $CBPQT^{4+}$ ion in the solution phase.

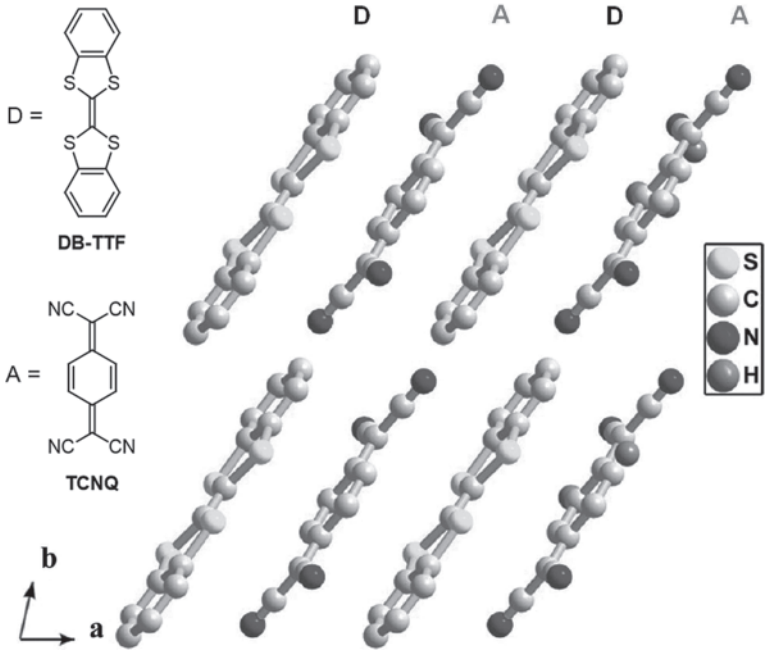

Figure 1.30 Formation of alternating D–A stacks of DB-TTF and TCNQ. (Reproduced from *CrystEngComm* 2014, *16*, 5968–5983).

1.4.6 Hydrophobic Effects

Hydrophobic effects play an important role in chemistry and biology. The term **hydrophobic** is derived from *hydro* (water) and *phobos* (fear), describing the tendency of nonpolar organic compounds (e.g., aliphatic hydrocarbons) toward aggregation when dispersed in water. The reason for these compounds to show **hydrophobicity** is not because they somewhat "fear" or repulsively interact with water molecules. Instead, hydrophobicity is a result of the differences between solvating water molecules and the bulk water molecules. In a solvation process, two energetic components come into play. The enthalpic (ΔH) effect describes the solvent/solute interactions, such as ion–dipole and dipole–dipole attractions. The entropic (ΔS) effect reflects the changes in the degree of ordering of solvent/solute molecules. As schematically illustrated in Figure 1.31, when individual molecules of a nonpolar compound (e.g., benzene) are dissolved in water, the molecular surface

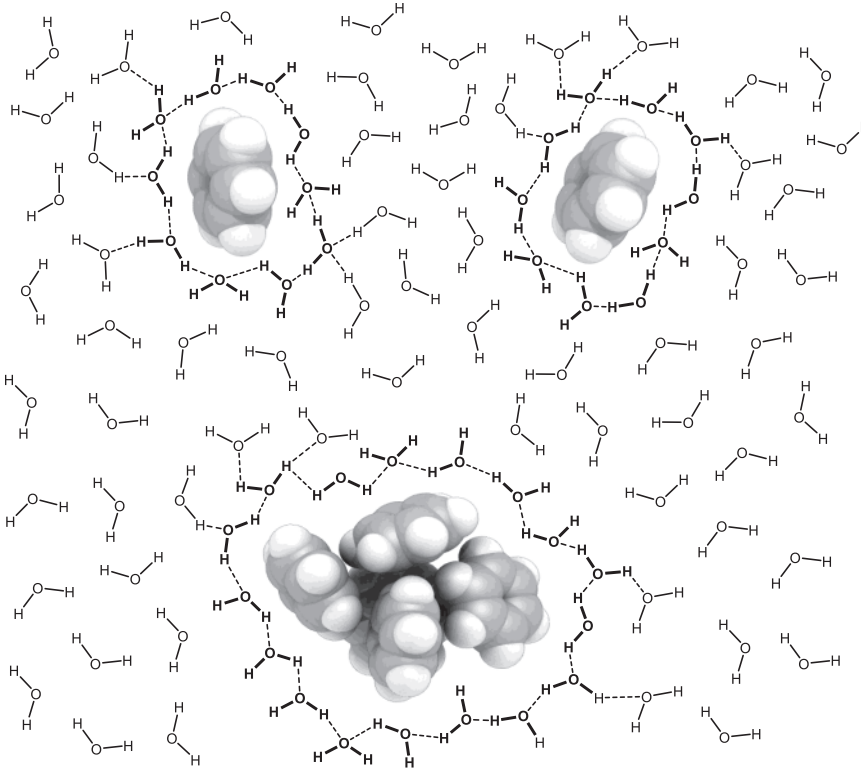

Figure 1.31 Water solvation of individual molecules and aggregates of benzene. Solvating water molecules (highlighted in bold) create cavities to host benzene molecules (solutes).

of each benzene molecule is surrounded by a cluster of water molecules to form a solvation shell, which in turn creates a cavity hosting the solute molecule. Water molecules in the solvation shell are organized in a rigid, quasi-crystalline structure, losing certain degrees of rotational and translational freedom. Therefore, the water molecules in the solvation shell are arranged in greater order than bulky water molecules. As a result, the total entropy of water as the solvent is decreased relative to its entropy before solvation. When benzene molecules approach one other to form aggregates, their effective surface area in contact with water is reduced, liberating some water molecules from the solvation shells. In other words, the number of ordered solvating water molecules per benzene is lowered, and consequently the entropy of water as the solvent is increased after aggregation of benzene. As discussed in Section 1.4.3 the water–benzene interaction is attractive with a strength equivalent to weak hydrogen bonding (i.e., the $\Delta H_{\text{solvent-solute}}$ term is a negative value). Nevertheless, the increase in the entropy term dominates the thermodynamics of benzene dispersion in water. The effect of the $T\Delta S_{\text{solvent}}$ term for non-aggregated benzene molecules is larger than the $\Delta H_{\text{solvent-solute}}$ term (ΔG positive) but smaller for aggregated benzene molecules (ΔG negative). Therefore, the aggregation of benzene molecules in water is a thermodynamically favored process.

Hydrophobicity can serve as an important driving force in guest–host chemistry. Figure 1.32 shows a class of compounds named cucurbit[*n*]urils, which are macrocycles of glycoluril linked through methylene linkages [40]. The nomenclature of cucurbiturils is derived from their resemblance to a pumpkin of the family of *Cucurbitaceae*. Cucurbit[*n*]urils are highly polar organic compounds with good water solubility. They possess a sufficiently large inner cavity to act as a molecular container to host a variety of neutral and cationic guest species in water. For example, cyclohexane can be encapsulated inside cucurbit[6]uril with an association constant (K_a) of 1300 M^{-1} in water at pH 3. Usually, the binding of a cucurbituril with a neutral molecule is driven by the hydrophobic effects, which entail the release of ordered water molecules from the inner cavity of the cucurbituril host and de-solvation of the neutral guest molecules. Cationic guests can also be trapped inside cucurbiturils through cation–dipole and CT interactions.

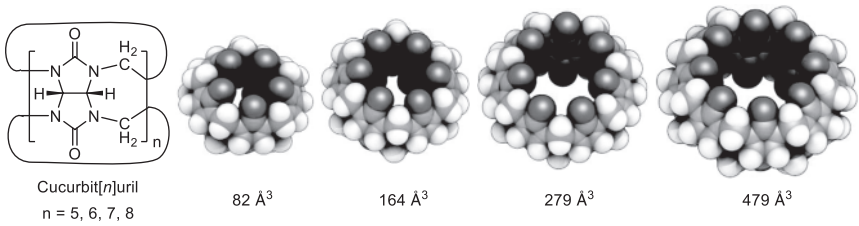

Figure 1.32 Molecular structures and CPK models and effective volumes of cucurbit[*n*]urils (*n* = 5–8).

1.5 Solvent Effects

Many chemical reactions and supramolecular assembling processes take place in a homogenous solution phase. The liquid component of a solution in the largest amount is called the **solvent**, while other substances in the solution are called **solutes**. Water is a "universal solvent" owing to its extremely large polarity ($\varepsilon = 80.1$ at 20 °C) and unique hydrogen bonding ability. In many chemical reactions, water is used to dissolve metal ions and polar compounds. In the biological world, water plays a life-sustaining role, supporting cellular structures and dictating the folding properties of amino acids, proteins, and DNA molecules to enable them to carry out their essential biological functions. Indeed, the impact of water as a solvent is so profound that we would generally classify solvents as **aqueous** or **nonaqueous**.

In the realm of organic chemistry, numerous nonaqueous solvents are used, since a large portion of organic compounds are hydrophobic and water insoluble [41]. Solvents can be classified by their physical and chemical properties. In general, liquids fall into three different classes, (1) molecular liquids, (2) ionic liquids, and (3) metals. Most of the commonly used liquid solvents used in chemical and biological applications are molecular liquids, which can be further classified as shown in Table 1.2.

Solvents play a vital role in organic reactions. As mentioned above, solvent molecules can interact with solute molecules in markedly different ways. The solvation effect of inert solvents (e.g., nonpolar alkanes) results in only minor changes in the structural and electronic properties of the solute molecules. Solvents with strong polarity and hydrogen bonding capability not only modify the properties of

Table 1.2 Classification of molecular solvents.

Classes	Properties	Examples
Inert	Unreactive, nonpolar, or weakly polar	Alkanes, fluorocarbons
Inert-polarizable	Electron pair donors, electron pair acceptors	Aromatic compounds, halogenated solvents, carbon disulfide, tetracyanoethane
Protogenic	Hydrogen bond donors	Acetic acid, sulfuric acid
Protophilic	Hydrogen bond acceptors	Tertiary amines
Amphiprotic	Having both hydrogen bond donor and acceptor capacity	Water, alcohols
Dipolar-aprotic	Have substantial dipole moments, but lack of marked hydrogen bond donor/acceptor capacity	Acetonitrile, DMF, DMSO, HMPA

solute molecules to a significant extent, but in some cases react with the solutes after dissolution. The solvent–solute reaction (i.e., solvolysis) changes the identity of the solute. Depending on the type of solvolysis reaction, a solvent molecule may act as a nucleophile or an electrophile and hence can strongly influence the kinetics and outcomes of the reaction. Take the S_N1 type of solvolysis of 2-admantyl triflate in water–ethanol mixtures as an example, the rate of solvolysis changes dramatically with the polarity of the mixture solvent (Figure 1.33A). An increase in the fraction of water from 20% to 80% leads to an acceleration of the reaction rate by three orders of magnitude. This dramatic solvent effect can be explained by the scheme illustrated in Figure 1.33B. The rate-limiting step of the S_N1 solvolysis is C–O bond breaking, yielding 2-adamantyl cation as the intermediate (IM). The transition state (TS) of this step bears a greater resemblance to the carbocation IM rather than the reactant, 2-adamantyl triflate. As discussed before, a cation–dipole interaction is stronger than a dipole–dipole interaction. It is therefore reasonable to deduce that in a polar medium, the solvation stabilization of the partially cationic TS is more pronounced than for the neutral reactant. As such, the energy barrier is lowered as the solvent polarity increases resulting in an increased solvolysis rate.

Solvolysis of various alkyl halides has been widely studied to evaluate the ability of the solvent to stabilize carbocations generated from a unimolecular rate-limiting step. Solvent effects also strongly influence other types of organic reactions. For example, if an S_N2 reaction uses an anion as the nucleophile, the reaction rate would be very slow in a protic solvent such as water or an alcohol, since the protic solvent molecules can act as hydrogen bond donors to strongly solvate the anion through hydrogen bonding interactions, which in turn reduce the nucleophilicity of the anion. The use of an aprotic dipolar solvent is preferred for such S_N2 reactions since it can sufficiently stabilize the transition state without compromising the reactivity of the anionic nucleophile. Solvents can also exert an

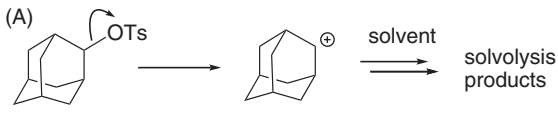

H_2O/EtOH (v:v)	k (s^{-1}, 25°C)
20 : 80	(1.70 ± 0.01) x 10^{-2}
50 : 50	(3.79 ± 0.09) x 10^{-2}
70 : 30	13 ± 3
80 : 20	22 ± 5

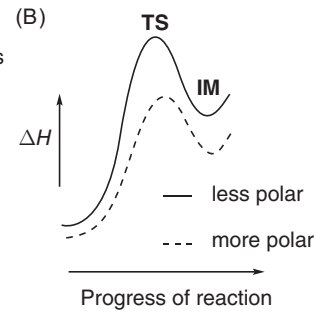

Figure 1.33 (A) Solvolysis of 2-admantyl triflate in mixtures of water and ethanol. Kinetic data are taken from *J. Org. Chem.* 1985, *50*, 4821–4823. (B) Schematic illustration of the solvent effects on the potential energy surface of the reaction.

important impact on acid–base exchange reactions. For example, the strength of a strong acid is limited or "leveled" by the basicity of the solvent. Similarly, the strength of a strong base is leveled by the acidity of the solvent. This is known as the **leveling effect**.

Solvent effects significantly influence CT interactions and related spectroscopic properties. As discussed before, the interactions of a donor (D) and an acceptor (A) molecule would lead to a CT complex, featuring a $D^{\delta+}\cdots A^{\delta-}$ type of charge separation. The stability of such a CT complex is solvent dependent. Polar solvents provide better stability for the CT complex than nonpolar solvents. The formation and properties of a CT complex can be probed by UV-Vis absorption analysis. In the UV-Vis absorption spectrum of a D···A complex, a new absorption band known as the **CT band** would emerge at a longer-wavelength position relative to the absorption bands of individual D and A molecules. The shape, intensity, and positions of UV-Vis absorption or fluorescence emission bands change as the nature of solvent is varied. This behavior is called **solvatochromism**. Monitoring the changes of the CT band of a chromophore in various solvents provides a quantitative way to assess solvent nature [42]. For example, the solvatochromic shifts of *N*-ethyl-4-methylcarboxypyridinium iodide (Figure 1.34A) in different solvents give the *Z*-scale for measuring solvent polarity. Herein *Z* is calculated by, $Z = 2.859 \times 10^4/\lambda_{max}$, where λ_{max} is the maximum absorption wavelength of the pyridinium iodide. Another popular set of solvatochromic parameters is called $E_T(30)$, which was first introduced by Reichardt et al. $E_T(30)$ is based on the electronic transition energy of a pyridinium-*N*-phenoxide dye (Figure 1.34B). The number 30 refers to the 30th candidate among numerous chromophores examined in their studies. The $E_T(30)$ scale can be expressed by the equation, $E_T(30) = 31.2 + 11.5\pi^* + 15.2\alpha$, where π^* reflects the polarizability and α describes the hydrogen bond-donating ability of the solvent.

Solvent effects are indispensable factors in supramolecular chemistry, especially in the formation of organized supramolecular self-assemblies through solvent-sensitive non-covalent forces such as hydrogen bonding, dipole–dipole interactions, and π–π stacking. Figure 1.35 shows an example of the solvophobically

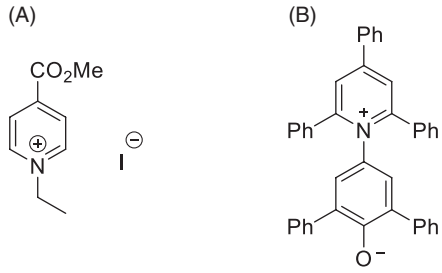

Figure 1.34 Two CT chromophores useful for evaluating solvent polarity.

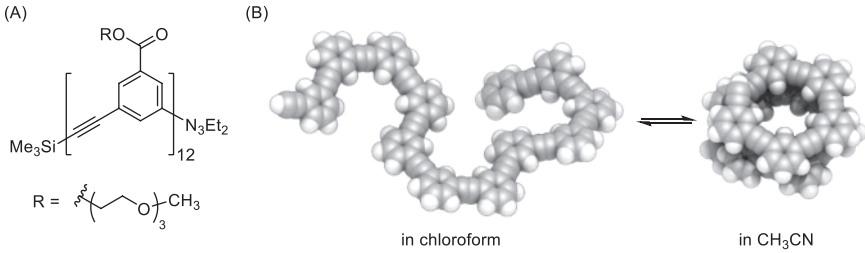

Figure 1.35 (A) Molecular structure and (B) the solvophobically driven conformational switching properties of an oligo(*m*-phenylene ethylene). Side chains and end groups are omitted in the illustration of molecular model for clarity.

driven folding of an oligomer of *m*-phenylene ethylene, which was synthesized and investigated by Moore and co-workers [43]. When dissolved in an appropriate solvent (chloroform), the oligomer prefers a random, disordered conformation. Upon switching to a more polar solvent (acetonitrile), the oligomer folds into a helical conformation, creating a cylindrical inner cavity that can be useful for hosting smaller guest species.

Further Reading

- Carey, F. A.; Sundberg, R. J., Advanced Organic Chemistry: Part A: Structure and Mechanisms. Springer Science & Business Media: 2007.
- Smith, M. B., March's Advanced Organic Chemistry: Reactions, Mechanisms, and Structure. John Wiley & Sons: 2020.
- Anslyn, E. V.; Dougherty, D. A., Modern Physical Organic Chemistry. University science books: 2006.
- Ozin, G. A.; Arsenault, A., Nanochemistry: A Chemical Approach to Nanomaterials. Royal Society of Chemistry: 2015.

References

1 Feynmann, R. P.; Leighton, R. B.; Sands, M., *The Feynmann Lectures on Physics*. Addison-Wesley: Reading, **1963**.
2 Taniguchi, N., On the Basic Concept of Nanotechnology. *Proc. of the ICPE*, Tokyo, **1974**, 18–23 .
3 Drexler, K. E., *Engines of Creation: The Coming Era of Nanotechnology*. Anchor Books: **1986**.
4 Lewis, G. N., The Atom and the Molecule. *J. Am. Chem. Soc*. **1916**, *38*, 762–785.
5 Gillespie, R. J.; Hargittai, I., *The VSEPR Model of Molecular Geometry*. Courier Corporation: **2013**.

6 Bader, R. F.; Gillespie, R. J.; MacDougall, P. J., A Physical Basis for the VSEPR Model of Molecular Geometry. *J. Am. Chem. Soc.* **1988**, *110*, 7329–7336.

7 Gillespie, R. J.; Robinson, E. A., Models of Molecular Geometry. *Chem. Soc. Rev.* **2005**, *34*, 396–407.

8 Cooper, D., *Valence Bond Theory*. Elsevier: Amsterdam, **2002**.

9 Pauling, L., The Nature of the Chemical Bond. Application of Results Obtained from the Quantum Mechanics and from a Theory of Paramagnetic Susceptibility to the Structure of Molecules. *J. Am. Chem. Soc.* **1931**, *53*, 1367–1400.

10 Pauling, L. C., The Theory of Resonance in Chemistry. *Proc. R. Soc.: Math. Phys. Sci.* **1977**, *356*, 433–441.

11 Gleiter, R.; Haberhauer, G., *Aromaticity and Other Conjugation Effects*. Wiley-VCH: Weiheim, **2012**.

12 Yates, K., *Hückel Molecular Orbital Theory*. Academic Press: New York, **1978**.

13 Krygowski, T. M.; Cyrański, M. K., Structural Aspects of Aromaticity. *Chem. Rev.* **2001**, *101*, 1385–1420.

14 Ho, T.-L., Hard Soft Acids Bases (HSAB) Principle and Organic Chemistry. *Chem. Rev.* **1975**, *75*, 1–20.

15 Pearson, R. G., Hard and Soft Acids and Bases. *J. Am. Chem. Soc.* **1963**, *85*, 3533–3539.

16 Mitchell, R. H., Measuring Aromaticity by NMR. *Chem. Rev.* **2001**, *101*, 1301–1316.

17 Chen, Z.; Wannere, C. S.; Corminboeuf, C.; Puchta, R.; Schleyer, P. V. R., Nucleus-Independent Chemical Shifts (NICS) as an Aromaticity Criterion. *Chem. Rev.* **2005**, *105*, 3842–3888.

18 Williams, R. V., Homoaromaticity. *Chem. Rev.* **2001**, *101*, 1185–1204.

19 Stahl, F.; Schleyer, P. v. R.; Jiao, H.; Schaefer, H. F.; Chen, K.-H.; Allinger, N. L., Resurrection of Neutral Tris-homoaromaticity. *J. Org. Chem.* **2002**, *67*, 6599–6611.

20 Rzepa, H. S., Möbius Aromaticity and Delocalization. *Chem. Rev.* **2005**, *105*, 3697–3715.

21 Ajami, D.; Oeckler, O.; Simon, A.; Herges, R., Synthesis of a Möbius Aromatic Hydrocarbon. *Nature* **2003**, *426*, 819–821.

22 Kawase, T.; Oda, M., Möbius Aromatic Hydrocarbons: Challenges for Theory and Synthesis. *Angew. Chem. Int. Ed.* **2004**, *43*, 4396–4398.

23 Yoon, Z. S.; Osuka, A.; Kim, D., Möbius Aromaticity and Antiaromaticity in Expanded Porphyrins. *Nat. Chem.* **2009**, *1*, 113--122.

24 Mulliken, R. S.; Rieke, C. A.; Brown, W. G., Hyperconjugation. *J. Am. Chem. Soc.* **1941**, *63*, 41–56.

25 Fleming, I., *Molecular Orbitals and Organic Chemical Reactions*. John Wiley & Sons: **2011**.

26 Alabugin, I. V.; Gilmore, K. M.; Peterson, P. W., Hyperconjugation. Wiley Interdiscip. *Rev. Comput. Mol. Sci.* **2011**, *1*, 109–141.

27 Alabugin, I. V.; Kuhn, L.; Krivoshchapov, N. V.; Mehaffy, P.; Medvedev, M. G., Anomeric Effect, Hyperconjugation and Electrostatics: Lessons from Complexity in a Classic Stereoelectronic Phenomenon. *Chem. Soc. Rev*. **2021**, *50*, 10212–10252.

28 von Ragué Schleyer, P.; Kos, A. J., The Importance of Negative (Anionic) Hyperconjugation. *Tetrahedron* **1983**, *39*, 1141–1150.

29 Garratt, P. J.; Ibbett, A. J.; Ladbury, J. E.; O'Brien, R.; Hursthouse, M. B.; Malik, K. A., Molecular Design Using Electrostatic Interactions. 1. Synthesis and Properties of Flexible Tripodand Tri-and Hexa-cations with Restricted Conformations. Molecular Selection of Ferricyanide from Ferrocyanide. *Tetrahedron* **1998**, *54*, 949–968.

30 Jeffrey, G. A., *An Introduction to Hydrogen Bonding*. Oxford University Press: New York, **1997**.

31 Bader, R. F., Atoms in Molecules. *Acc. Chem. Res*. **1985**, *18*, 9–15.

32 Arunan, E.; Desiraju, G. R.; Klein, R. A.; Sadlej, J.; Scheiner, S.; Alkorta, I.; Clary, D. C.; Crabtree, R. H.; Dannenberg, J. J.; Hobza, P., Definition of the Hydrogen Bond (IUPAC Recommendations 2011). *Pure Appl. Chem*. **2011**, *83*, 1637–1641.

33 Martinez, C. R.; Iverson, B. L., Rethinking the Term "Pi-stacking." *Chem. Sci*. **2012**, *3*, 2191–2201.

34 Hunter, C. A.; Sanders, J. K., The Nature of π-π Interactions. *J. Am. Chem. Soc*. **1990**, *112*, 5525–5534.

35 Pérez, E. M.; Martín, N., π–π Interactions in Carbon Nanostructures. *Chem. Soc. Rev*. **2015**, *44*, 6425–6433.

36 Soteras, I.; Orozco, M.; Luque, F. J., Induction Effects in Metal Cation–Benzene Complexes. *Phys. Chem. Chem. Phys*. **2008**, *10*, 2616–2624.

37 Stone, A., *The Theory of Intermolecular Forces*. 2nd ed.; Oxford University Press: Oxford, UK, **2013**.

38 Das, A.; Ghosh, S., Supramolecular Assemblies by Charge-Transfer Interactions between Donor and Acceptor Chromophores. *Angew. Chem. Int. Ed*. **2014**, *53*, 2038–2054.

39 Jiang, H.; Yang, X.; Cui, Z.; Liu, Y.; Li, H.; Hu, W.; Kloc, C., Adjusting Tetrathiafulvalene (TTF) Functionality through Molecular Design for Organic Field-Effect Transistors. *Cryst. Eng. Comm*. **2014**, *16*, 5968–5983.

40 Isaacs, L., Cucurbit[n]urils: From Mechanism to Structure and Function. *Chem. Commun*. **2009**, 619–629.

41 Reichardt, C.; Welton, T., *Solvents and Solvent Effects in Organic Chemistry*. John Wiley & Sons: Weinheim, **2011**.

42 Reichardt, C., Solvatochromic Dyes as Solvent Polarity Indicators. *Chem. Rev*. **1994**, *94*, 2319–2358.

43 Nelson, J. C.; Saven, J. G.; Moore, J. S.; Wolynes, P. G., Solvophobically Driven Folding of Nonbiological Oligomers. *Science* **1997**, *277*, 1793–1796.